A Novel Theoretical Approach to the Analysis of Dendritic Transients

Hagai Agmon-Snir
Department of Neurobiology, Institute of Life Sciences, Hebrew University, Jerusalem 91904, Israel, and Mathematical Research Branch, NIDDK, National Institutes of Health, Bethesda, Maryland 20892

ABSTRACT A novel theoretical framework for analyzing dendritic transients is introduced. This approach, called the method of moments, is an extension of Rall's cable theory for dendrites. It provides analytic investigation of voltage attenuation, signal delay, and synchronization problems in passive dendritic trees. In this method, the various moments of a transient signal are used to characterize the properties of the transient. The strength of the signal is measured by the time integral of the signal, its characteristic time is determined by its centroid ("center of gravity"), and the width of the signal is determined by a measure similar to the standard deviation in probability theory. Using these signal properties, the method of moments provides theorems, expressions, and efficient algorithms for analyzing the voltage response in arbitrary passive trees. The method yields new insights into spatiotemporal integration, coincidence detection mechanisms, and the properties of local interactions between synaptic inputs in dendritic trees. The method can also be used for matching dendritic neuron models to experimental data and for the analysis of synaptic inputs recorded experimentally.

GLOSSARY

t	time (s)
x, y, z	points in a passive structure
$V(x, t)$	transmembrane voltage at point x relative to resting potential (V)
$I(x, t)$	input current density applied at point x (A/cm)
R_m	specific membrane resistivity (Ω·cm^2)
R_i	specific axial resistivity (Ω·cm)
C_m	specific membrane capacitance (F/cm^2)
r_m	membrane resistance of a unit length of a cylinder (Ω·cm)
r_i	axial resistance per unit length of a cylinder (Ω/cm)
λ	space constant of a cylinder (cm)
τ	time constant of a passive membrane (s)
X	electrotonic distance along a cylinder
L	electrotonic length of a cylinder
T	t/τ
R_∞	r_m/λ for a given cylinder (Ω)
$f(t)$	a transient signal
$m_{f,i}$	ith moment of a transient signal $f(t)$
$\tilde{f}(s)$	Laplace transform of a signal $f(t)$
$\hat{s}_f$	strength of a transient signal $f(t)$
$\hat{\imath}_f$	characteristic time of a transient signal $f(t)$ (s)
$\hat{w}_f^2$	dispersion of a transient signal $f(t)$ (s^2)
$\hat{w}_f$	width of a transient signal $f(t)$ (s)
$\hat{k}_f$	skewness of a transient signal $f(t)$
$\vec{\square}$	an arrow above a symbol indicates a directional property
$R_{in}(x)$	input resistance at point x (Ω)
$G_{in}(x)$	input conductance at point x (Siemens)
$R_{tr}(y, x)$	transfer resistance between points y and x (Ω)
$A(y, x)$	attenuation factor between points y and x
$\vec{A}_r(x)$	attenuation rate at point x in a given direction (cm^{-1})
$D_{tr}(y, x)$	transfer delay between points y and x (s)
$D_{in}(x)$	input delay at point x (s)
$PD(y, x)$	propagation delay between points y and x (s)
$\vec{\theta}(x)$	velocity at point x in a given direction (cm/s)
$B_{tr}(y, x)$	transfer broadening between points y and x (s^2)
$B_{in}(x)$	input broadening at point x (s^2)
$PB(y, x)$	propagation broadening between points y and x (s^2)
$\vec{B}_r(x)$	broadening rate at point x in a given direction (s^2/cm)
$i(t)$	an input signal to a system
$o(t)$	an output response of a system
$G(t)$	Green's function for a continuous time-invariant linear system
$H(s)$	transfer function of a continuous time-invariant linear system
$\tilde{R}_{in}(x, s)$	input impedance at point x
$\tilde{G}_{in}(x, s)$	input admittance at point x
$\tilde{R}_L(s)$	input impedance of a passive dendritic load
R_L	input resistance of a passive dendritic load (Ω)
D_L	input delay of a passive dendritic load (s)
B_L	input broadening of a passive dendritic load (s^2)
$\tilde{\lambda}_{eff}(x)$	effective λ at point x in a given direction (cm)
$\tau_{eff}(x)$	effective τ at point x (s)
$\eta(x)$	$B_{in} - (D_{in})^2$ (s^2)

Received for publication 31 October 1994 and in final form 17 July 1995.

Address reprint requests to Dr. Hagai Agmon-Snir, Mathematical Research Branch, NIDDK, BSA, 9190 Wisconsin Avenue, Suite 350, Bethesda, MD 20814-3800. Tel.: 301-496-4325; Fax: 301-402-0535; E-mail: hagai@helix.nih.gov.

0006-3495/95/11/1633/00 $2.00

INTRODUCTION

Our present insights regarding the computational function of single nerve cells are heavily based on Rall's passive cable theory for dendrites (for reviews, see Rall, 1959, 1977, 1989; Jack et al., 1983; McKenna et al., 1992; Segev, 1992, 1995; Mel, 1994; Segev et al., 1994). The mathematical methods derived by Rall and extended by others (reviewed in Rall, 1977, 1989; Jack et al., 1983; Tuckwell, 1988; and see below) enable one to compute the time course of the voltage response at any point, $V(x,t)$, to transient current inputs injected to arbitrary passive trees. One method is the compartmental modeling approach, which, for complicated trees, requires time-consuming computer simulations (Rall, 1964; Segev et al., 1989; Hines, 1989; Rapp et al., 1994). Other methods are based on analytical evaluation of the Laplace transform of the voltage response and then numerical reverse-transformation of the result to the time domain (Butz and Cowan, 1974; Horwitz, 1981; Koch and Poggio, 1985; Holmes, 1986). An alternative approach is to express the voltage response as an infinite sum of

expressions that converges quickly for early times (Abbott et al., 1991; Cao and Abbott, 1993) or at late times (Major al., 1993). Another approach is to simplify the geometry of the tree to an equivalent structure (e.g., Rall, 1962b; Rall and Rinzel, 1973; Whitehead and Rosenberg, 1993). In some cases, the voltage response can be expressed in a straightforward manner and analyzed analytically (Durand, 1984; Kawato, 1984).

Utilizing these methods, realistic models of reconstructed trees of various types have been built and explored (see review in Segev, 1992). These models showed the interplay between dendritic morphology, electrical properties, spatio-temporal distribution of synapses, and the input-output properties of neurons. In addition, matching the predictions of these models to corresponding experimental results (e.g., Brown et al., 1981; Fleshman et al., 1988; Clements and Redman, 1989; Stratford et al., 1989; Rapp et al. 1994; Major et al., 1994) has yielded estimates for the biophysical parameters (e.g., specific membrane resistivity, R_m, specific membrane capacitance, C_m, and cytoplasm resistivity, R_i).

In this paper we suggest an alternative, general approach for characterizing and analyzing dendritic transients. Rather than computing the whole time course of the voltage response, a few selected properties of the transient current and voltage response are computed analytically. These properties are defined using the moments of the transient signal. As a result, much of the analysis becomes general and independent of the input shape. The analysis yields mathematical theorems and analytic expressions that govern the voltage response in an arbitrarily shaped passive dendritic tree. The most important moments-based properties of a dendritic transient signal are depicted in Fig. 1 and are interpreted as the strength of the signal, $\hat{s}_f$, its characteristic time, $\hat{t}_f$, and its width, $\hat{w}_f$ (or dispersion, $\hat{w}_f^2$). Other measures, e.g., the skewness of the signal, $\hat{k}_f$, can also be derived.

Mathematically, the moments-based approach is an extension of the steady-state passive cable theory to the transient case. It provides a generalization for the classical definitions of the space constant (λ) and the time constant (τ). These generalized definitions provide new insights into the rate of attenuation and the velocity of transient signals in passive structures. These parameters can be further extended for certain nonlinear cases (in preparation).

The method of moments is a tool for exploring the spatio-temporal integration properties in dendrites. It may provide answers and insights for questions as, What is the time delay of the transient signals in trees with arbitrary branching? How does this delay depend on the biophysical parameters of the tree? What is the width of the time window for synaptic integration or coincidence detection at various dendritic locations? What is the dendritic domain of the synapses that may affect a target point in the dendrites? These questions were explored previously using the classical properties of the voltage response: the time to peak, the half-width, and the 10–90% rise time (Rall, 1967; Rall et al., 1967; Jack and Redman, 1971; Redman, 1973; Barrett and Crill, 1974; and review in Rall et al., 1992). The classical properties can be analyzed by numerical methods, the results of which are specific for the parameters of the model (input shape, biophysical and geometrical properties of the dendritic tree). The generality of the method of moments provides more general answers, in much less computation time.

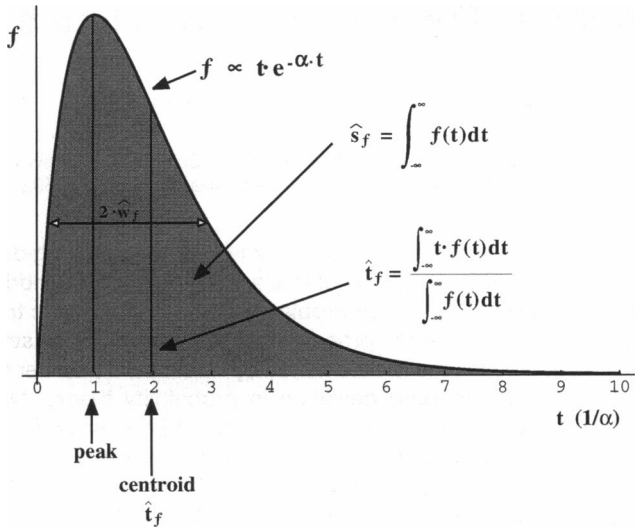

FIGURE 1 Definitions of strength, characteristic time, and width of a signal. In this figure, a transient signal with a shape of an α-function, i.e., $f(t) \propto t \cdot \exp(-\alpha t)$, is depicted. The shaded area under the function is the signal strength, $\hat{s}_f$. The centroid of the signal is the signal characteristic time, $\hat{t}_f$. Because the signal width, $\hat{w}_f$, is analogous to the standard deviation in probability theory, $2 \cdot \hat{w}_f$ is shown in the graph. As discussed in the text, the width is useful when comparing two signals. The peak point of the signal, which is classically used for characterizing the signal, is also shown as a reference.

The paper starts with moments-based definitions of various properties of transient signals in dendritic trees. The method of moments is then introduced and the relationship between the moments and the Laplace transform is expressed mathematically. General theorems, analytic expression, and algorithms for analyzing attenuation, delay, and broadening of transient signals in arbitrary passive trees are derived. In the Discussion, the functional interpretation of the moments-based properties is elaborated. The method of moments was used for a detailed analysis of dendritic delays in passive structures in Agmon-Snir and Segev (1993) and for the analysis of signal width in Agmon-Snir (1994). It was also used in conjunction with morphoelectrotonic transforms of dendritic trees in Zador et al. (1995).

DEFINITIONS

Except when otherwise specified, all of the models in this work are for passive dendritic trees with transient current inputs. The application of the results to nonlinear dendritic trees and to conductance change inputs is discussed in the Discussion. In this work, a passive dendritic tree is composed of cylinders and isopotential components (e.g., soma,

dendritic spine head). Each cylinder obeys the one-dimensional cable equation,

$$\lambda^2 \cdot \frac{\partial^2 V(x,t)}{\partial x^2} - \tau \cdot \frac{\partial V(x,t)}{\partial t} - V(x,t) = -r_m \cdot I(x,t) \qquad (1)$$

The time constant (τ) and the space constant (λ) may vary in different parts of the tree, but all parts have the same resting potential, which is assumed to be zero. The boundary conditions of each cylinder may be sealed end, leaky end, clamped to resting potential, or a connection to other segments in the tree. These assumptions are important to guarantee that the voltage response (V) to a transient current injection (I) will also be transient. The results in this work may be applied to other passive structures, e.g., tapering cables.

Moments

Let $f(t)$ be a transient signal. The ith moment of $f(t)$, $m_{f,i}$ ($i = 0, 1, 2, \cdots$), is

$$m_{f,i} \equiv \int_{-\infty}^{\infty} t^i \cdot f(t)\, dt \qquad (2)$$

In this work we require that all moments of $f(t)$ exist and that for every i ($i = 0, 1, 2, \cdots$),

$$\lim_{t \to \pm\infty} t^i \cdot f(t) = 0 \qquad (3)$$

It is easy to see that in practice, all experimental transient currents meet these requirements. In passive structures, the voltage response at any point meets these requirements. In some of the definitions below it is also required that the zeroth moment of the signals will not be equal to 0. This requirement is met if the total injected charge is not 0.

Moments-based properties of a transient signal

The properties of a transient signal, $f(t)$, are defined here using the moments of the signal. The definitions of strength, characteristic time, and width of a signal are illustrated in Fig. 1.

The strength of the signal, $\hat{s}_f$, is $m_{f,0}$, i.e., the time-integral of the signal, $\int_{-\infty}^{\infty} f(t)\, dt$. For current signals, the strength is the total injected charge.

The characteristic time of the signal, $\hat{t}_f$, is

$$\hat{t}_f \equiv \frac{m_{f,1}}{m_{f,0}} = \frac{m_{f,1}}{\hat{s}_f} \qquad (4)$$

$\hat{t}_f$ has an interpretation of "center of gravity" (centroid) of $f(t)$ in the following sense:

$$\int_{-\infty}^{\infty} (t - \hat{t}_f) \cdot f(t)\, dt = 0 \qquad (5)$$

The dispersion of the signal, $\hat{w}_f^2$, is

$$\hat{w}_f^2 \equiv \int_{-\infty}^{\infty} (t - \hat{t}_f)^2 \cdot \frac{f(t)}{\hat{s}_f}\, dt = \frac{m_{f,2}}{\hat{s}_f} - \hat{t}_f^2 \qquad (6)$$

The definition of dispersion is similar to the definition of the variance in probability theory. It is a measure of the dispersion of the signal around the centroid. The width of the signal, $\hat{w}_f$, is defined as the square root of $\hat{w}_f^2$, similar to the definition of standard deviation in probability theory. It is another measure of the signal dispersion, with units of time.

The skewness of the signal, $\hat{k}_f$, is

$$\hat{k}_f \equiv \int_{-\infty}^{\infty} \left(\frac{t - \hat{t}_f}{\hat{w}_f}\right)^3 \cdot \frac{f(t)}{\hat{s}_f}\, dt = \frac{m_{f,3} - 3 \cdot \hat{t}_f \cdot m_{f,2} + 2 \cdot \hat{t}_f^3 \cdot \hat{s}_f}{\hat{s}_f \cdot \hat{w}_f^3}$$
$$= \frac{m_{f,3}}{\hat{s}_f \cdot \hat{w}_f^3} - \frac{3 \cdot \hat{t}_f}{\hat{w}_f} - \frac{\hat{t}_f^3}{\hat{w}_f^3} \qquad (7)$$

As in probability theory, the skewness is a measure of asymmetry. It is exactly 0 for symmetrical signals. It is positive if the signal is skewed to the positive (right) side of the centroid and it is negative if the signal is skewed to the negative side of the centroid. The skewness will not be treated further in this article, but the same methods used here can also be applied for its analysis. Other shape properties of $f(t)$ can also be defined using moments, simply by using a higher power in the integral in Eq. 7. For example, using the power 4, we get the kurtosis of the signal.

Properties of the voltage response and corresponding definitions

The concept of directional property at a point

Some of the properties defined in this article are attributes of a point in a structure. $G_{in}(y)$, the input conductance at point y in a passive structure, is an example of such a property. Some other properties are attributes of a point in a structure and a given direction from it. Such properties are called here directional properties, and they are denoted by an arrow above their symbol (these properties are *not* vectors!). If we consider, for example, a branch point y in a dendritic structure, there are three directions for current flow from this point. For every such direction, the directional input conductance, denoted by $\vec{G}_{in}(y)$, is defined as the input conductance of the structure in this direction (when the other structures are substituted by sealed ends). The mathematical relation between $G_{in}(y)$ at the branch point and the directional input conductances is $G_{in}(y) = \vec{G}_{in,1}(y) + \vec{G}_{in,2}(y) + \vec{G}_{in,3}(y)$, where $\vec{G}_{in,1}(y)$, $\vec{G}_{in,2}(y)$, $\vec{G}_{in,3}(y)$ are the various directional input conductances at point y. In the case of a soma coupled to a cylinder, there are two directional input conductances at the soma point: one is the input conductance of the soma alone and the second is the input conductance of the cylinder at the connection point.

Another example of a directional property is the directional space constant $\vec{\lambda}$. At a branch point there are three directional space constants, which are the space constants of the three cylindrical segments that are connected to this point. In the case of a soma connected to a dendritic tree, there is only one directional space constant at the soma point.

Resistance and signal attenuation

Classically, the input resistance, transfer resistance, attenuation factor, and attenuation rate are defined for the steady-state case, using the steady-state values of the injected current and the voltage response. For the transient case, analogous definitions, using the strengths of the signals instead of the steady-state values, can be used. In passive structures, these analogous definitions for the transient case have the same values as the corresponding definitions for the steady-state case (Rinzel and Rall, 1974; see Strength, Resistance, and Attenuation for Transient Signals, below). Hence, when a transient current input is injected at point y in a tree, the input resistance at this point, $R_{in}(y)$, is the ratio between the strength of the transient voltage response at point y, $\hat{s}_V(y)$, and the strength of the current input, $\hat{s}_I(y)$. Transfer resistance, $R_{tr}(y, x)$, is the ratio between the strength of the transient voltage response at a given location in the structure (x) and the strength of the current input at the injection point (y). If the current flows in the structure from point y to point x, the attenuation factor between these points, $A(y, x)$, is the ratio between the strength of the transient voltage response at point y and the strength of the voltage response at point x (note that $A(y, x) \geq 1$ in passive structures). These definitions are illustrated in Fig. 2. The attenuation rate of the voltage response at point x_0 in a given direction, $\vec{A}_r(x_0)$, is the relative rate of the change in the strength of the voltage response, $\hat{s}_V(x)$, at this point, when the signal propagates in the given direction,

$$\vec{A}_r(x_0) \equiv \left|\frac{d\hat{s}_v(x)/dx}{\hat{s}_v(x)}\right|_{x=x_0} = \left|\frac{d\ \ln(\hat{s}_v(x))}{dx}\right|_{x=x_0} \quad (8)$$

where the derivative is in the direction of interest.

Delay

Delay is defined using the difference between the characteristic times of two signals. Accordingly, three types of delay are defined. Transfer delay is defined as $D_{tr}(y, x) = t_V(x) - t_I(y)$, where $\hat{t}_I(y)$ is the characteristic time of the transient current input at the injection point y, and $\hat{t}_V(x)$ is the characteristic time of the voltage response at x. Input delay, $D_{in}(y)$, is defined as $D_{tr}(y, y)$. (In Agmon-Snir and Segev (1993) and in Agmon-Snir (1994), the term *local delay* is also used for the input delay and the term *total delay* is also used for the transfer delay.) Propagation delay is then defined as $PD(y, x) = \hat{t}_V(x) - \hat{t}_V(y)$, where y and x are points in the structure, and the current flows from y to x. These definitions are depicted in Fig. 2. The velocity, or

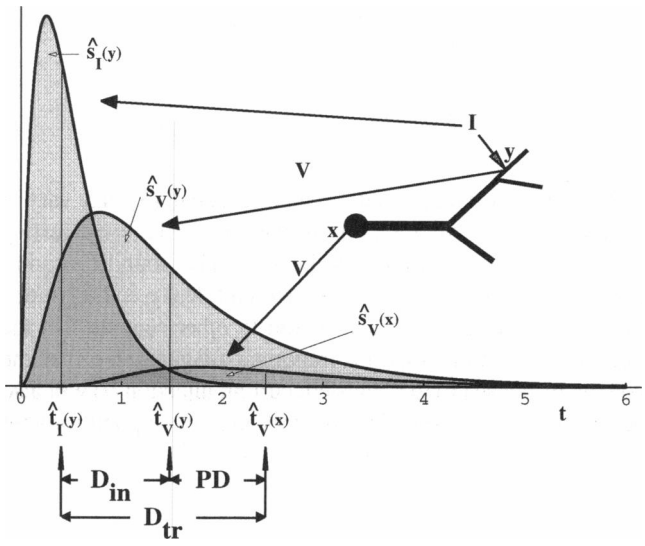

FIGURE 2 Resistance, attenuation, and delay definitions. In this scheme, a transient (α-function shaped) current is injected at point y in a passive structure, and the voltage responses at y and at another location x are depicted. The shaded areas below the functions show the strengths of the various signals. The input resistance, $R_{in}(y)$, is defined as $\hat{s}_V(y)/\hat{s}_I(y)$; the transfer resistance, $R_{tr}(y, x)$, is $\hat{s}_V(x)/\hat{s}_I(y)$; and the attenuation factor, $A(y, x)$, is $\hat{s}_V(y)/\hat{s}_V(x)$. The vertical lines show the characteristic times of the various signals. The input delay, $D_{in}(y)$, is defined as $\hat{t}_V(y) - \hat{t}_I(y)$; the transfer delay, $D_{tr}(y, x)$, is $\hat{t}_V(x) - \hat{t}_I(y)$; and the propagation delay, $PD(y, x)$, is $\hat{t}_V(y) - \hat{t}_V(x)$.

speed of propagation, of the voltage response at a point x_0 in a given direction, $\vec{\theta}(x_0)$, is defined as the reciprocal of the rate of the change in $\hat{t}_V(x)$ at this point, when the signal propagates in the given direction,

$$\vec{\theta}(x_0) \equiv \left|\left(\frac{d\hat{t}_v(x)}{dx}\right)^{-1}\right|_{x=x_0} \quad (9)$$

where the derivative is in the direction of interest.

Broadening

We define broadening using the difference between the dispersions of two signals. Accordingly, three types of broadening are defined. Transfer broadening, $B_{tr}(y, x)$, is

$$B_{tr}(y, x) \equiv \hat{w}_v^2(x) - \hat{w}_I^2(y) \quad (10)$$

where $\hat{w}_I^2(y)$ is the dispersion of the current at the input point y and $\hat{w}_V^2(x)$ is the dispersion of the voltage response at point x. Similar to the definitions of input resistance and input delay, the input broadening is defined as $B_{in}(y) = B_{tr}(y, y)$. Propagation broadening, $PB(y, x)$, is

$$PB(y, x) \equiv \hat{w}_v^2(x) - \hat{w}_v^2(y) \quad (11)$$

The broadening rate of the voltage response at a point x_0 in a given direction, $B_r(x_0)$, is the rate of the change in $\hat{w}_V^2(x)$ at this point, when the signal propagates in the

given direction,

$$\vec{B}_r(x_0) \equiv \left|\frac{d\hat{w}_v^2(x)}{dx}\right|_{x=x_0} \tag{12}$$

where the derivative is in the direction of interest.

THE METHOD OF MOMENTS

The method of moments utilizes the moments-based properties of transient signals for analyzing input-output relations in time-invariant linear systems. Passive dendritic structures, as defined above, are continuous time-invariant linear systems where, in our case, the input is an injected current and the output is a voltage response. A common way for representing the input-output properties of continuous time-invariant linear systems is by using Laplace transforms (Neff, 1984), and in many interesting cases it is easy to find an analytic expression for the Laplace transform of the output, when the Laplace transform of the input is known. For a continuous time-invariant linear system, the ratio between the Laplace transform of the output and the Laplace transform of the input is the same for all inputs and is called the transfer function of the system. This relation is expressed:

$$\tilde{o}(s) = \tilde{i}(s) \cdot H(s) \tag{13}$$

where $\tilde{i}(s)$ is the Laplace transform of the input signal $i(t)$, $\tilde{o}(s)$ is the Laplace transform of the output response $o(t)$, and $H(s)$ is the transfer function. $H(s)$ is the Laplace transform of the Green's function, $G(t)$, for this system (i.e., the impulse-response function). The Laplace transform of a signal $f(t)$ is defined as

$$\tilde{f}(s) \equiv \int_{-\infty}^{\infty} e^{-st} \cdot f(t)\, dt \tag{14}$$

(In many applied mathematics books, the Laplace transform is defined using 0 as the lower limit of the integral instead of ∞. This right-sided definition assumes that $f(t) = 0$ for $t < 0$.)

The relation between the Laplace transform of $f(t)$ and its moments is given by

$$m_{f,i} \equiv \int_{-\infty}^{\infty} t^i \cdot f(t)\, dt = \left[(-1)^i \cdot \frac{d^i}{ds^i}\tilde{f}(s)\right]_{s=0} \tag{15}$$

The moments theorem

In a continuous time-invariant linear system with a transient input, the ith moment of the output response depends only on the zeroth, first, . . . , ith moments of the input signal and of the Green's function.

Proof: Differentiating i times both sides of Eq. 13, we get on the right side an expression that contains the zeroth, first, . . . , ith derivatives of H and $\tilde{i}$. On the left side we get the ith derivative of $\tilde{o}$. If we set $s = 0$ on both sides and using Eq. 15, we find an expression for the ith moment of the output signal, which contains only the zeroth, first, . . . , ith moments of the input signal and the zeroth, first, . . . , ith moments of the Green's function. This completes the proof.

This theorem is useful for proving the theorems regarding the properties of the response function (see below).

The moments equations

In passive structures, equations for the moments of the voltage response are derived using Eq. 1. We define $Q_i \equiv V \cdot t^i$ ($i = 0, 1, 2, \cdots$), and rewrite the cable equation,

$$\lambda^2 \cdot \frac{\partial^2}{\partial x^2}\left(\frac{Q_i(x,t)}{t^i}\right) - \tau \cdot \frac{\partial}{\partial t}\left(\frac{Q_i(x,t)}{t^i}\right) - \left(\frac{Q_i(x,t)}{t^i}\right) = -r_m \cdot I(x,t) \tag{16}$$

Expanding the second term on the left side using the basic rules of differentiation (distinguishing between the case of $i = 0$ and positive i), multiplying the equation by t^i and then integrating both sides, we get

$$\lambda^2 \cdot \int_{-\infty}^{\infty} \frac{\partial^2 V(x,t)}{\partial x^2}\, dt - \tau \cdot \int_{-\infty}^{\infty} \frac{\partial V(x,t)}{\partial t}\, dt - \int_{-\infty}^{\infty} V(x,t)\, dt = -r_m \cdot \int_{-\infty}^{\infty} I(x,t)\, dt \tag{17}$$

for $i = 0$, whereas for positive i,

$$\lambda^2 \cdot \int_{-\infty}^{\infty} \frac{\partial^2}{\partial x^2} Q_i(x,t)\, dt - \tau \cdot \int_{-\infty}^{\infty} \frac{\partial}{\partial t} Q_i(x,t)\, dt + i \cdot \tau \cdot \int_{-\infty}^{\infty} Q_{i-1}(x,t)\, dt - \int_{-\infty}^{\infty} Q_i(x,t)\, dt = -r_m \cdot \int_{-\infty}^{\infty} t^i \cdot I(x,t)\, dt \tag{18}$$

Under the assumption of Eq. 3, the second term on the left in Eqs. 17 and 18 is zero. Interchanging the order of integration and derivation in the leftmost term in Eqs. 17 and 18, and using the moments definitions, we finally get the moments equations,
for $i = 0$,

$$\lambda^2 \cdot \frac{d^2}{dx^2} m_{v,0}(x) - m_{v,0}(x) = -r_m \cdot m_{I,0}(x) \tag{19}$$

and for positive i,

$$\lambda^2 \cdot \frac{d^2}{dx^2} m_{v,i}(x) - m_{v,i}(x) = -r_m \cdot m_{I,i}(x) - i \cdot \tau \cdot m_{v,i-1}(x) \quad (20)$$

Equation 19 was derived by Rinzel and Rall (1974) in the context of the time integral of transients. They showed, using the similarity between Eq. 19 and the steady-state cable equation, that in a given passive tree, the area under the transient voltage (the zeroth moment) attenuates like the steady-state voltage, independent of the shape of the voltage transient (see below).

In solving the moments equations for a particular case, the boundary conditions can be easily derived from the corresponding boundary conditions for the cable equation (Eq. 1). Using the moments equations, which are ordinary differential equations with constant coefficients similar to the steady-state cable equation, an algorithm for computing moments in passive dendrites with arbitrary branching structure can be derived. This algorithm is similar to the recursive algorithm suggested by Rall (1959) for computing steady voltage attenuation in such trees. However, we will not use the moments equations in this article. Instead, we will analyze signal properties (e.g., the strength, the characteristic time, the width of the signal) directly, using the properties of the Laplace transform and its relation to the signal moments (Eq. 15).

PROPERTIES OF THE LAPLACE TRANSFORM IN PASSIVE STRUCTURES

The following properties of the Laplace transform in the context of passive dendritic trees are discussed in detail elsewhere (Rall, 1960; Butz and Cowan, 1974; Koch et al., 1982; Tuckwell, 1988). Here we highlight only those relevant to this paper.

The Laplace transform of the cable equation, Eq. 1, is

$$\left(\frac{\lambda}{(1 + \tau \cdot s)^{1/2}}\right)^2 \cdot \frac{\partial^2 \tilde{V}(x, s)}{\partial x^2} - \tilde{V}(x, s) = -\frac{r_m}{1 + \tau \cdot s} \cdot \tilde{I}(x) \quad (21)$$

which is similar to the steady-state cable equation,

$$\lambda^2 \cdot \frac{d^2 V(x)}{dx^2} - V(x) = -r_m \cdot I(x) \quad (22)$$

Also, the boundary conditions can be found easily in the Laplace domain and, again, they are very similar to the corresponding conditions in the steady-state case.

The properties of the voltage response in the Laplace domain are analogous to the properties of the steady-state voltage response. The latter are discussed in detail in Rall (1977, 1989), Jack et al. (1983), and Tuckwell (1988). In the following, the properties of the Laplace transform in passive dendritic structures are stated without proof.

Linearity

If $\tilde{V}_1(x, s)$ is a response to the input $\tilde{I}_1(y_1, s)$, and if $\tilde{V}_2(x, s)$ is a response to the input $\tilde{I}_2(y_2, s)$, $\tilde{V}_1(x, s) + \tilde{V}_2(x, s)$ is the response to the input $\tilde{I}_1(y_1, s) + \tilde{I}_2(y_2, s)$.

Reciprocity

Given two points (y,x) in a passive structure, if a current $\tilde{I}(s)$ is injected at point y and the resultant voltage response at point x is $\tilde{V}(s)$, then if the same current, $\tilde{I}(s)$, is injected at point x, the resultant voltage response at point y is $\tilde{V}(s)$.

Input invariance

The ratio between a current $\tilde{I}(s)$ injected at a point y in a passive structure, and the voltage response, $\tilde{V}(s)$, at point x in the structure depends only on the details of the structure and on the two points, and is independent of $\tilde{I}(s)$. When $x = y$, the ratio $\tilde{I}(s)/\tilde{V}(s)$ is defined as the input admittance at point y and is denoted by $\tilde{G}_{in}(y, s)$. The input impedance at this point is $\tilde{R}_{in}(y, s) = 1/\tilde{G}_{in}(y, s)$. The input admittance and the input impedance match the corresponding definitions in electricity theory when $s = i \cdot \omega$, and ω is the angular frequency ($i = \sqrt{-1}$).

Equivalent boundary condition for a tree

When a passive dendritic tree is connected at the end of a cylinder, then the boundary condition at this end can be described by the input impedance $\tilde{R}_{in}(s)$ of this dendritic tree at the point of connection (in other words, by $\tilde{R}_{in}(s)$ at the connection point in the direction of the dendritic tree). In this context, we refer to the impedance of the dendritic tree at the boundary as the dendritic load at the end of the cylinder, denoted by $\tilde{R}_L(s)$. Algorithms for computing Laplace transform in arbitrary dendritic trees that make use of this property can be found in Butz and Cowan (1974), Horwitz (1981), Koch and Poggio (1985), and Holmes (1986).

Expressions for calculating Laplace transform response in a cylinder

Consider the case when a dendritic load, $\tilde{R}_L(s)$, is connected at one end of a cylinder (at $X = L$), and the other end of this cylinder (at $X = 0$) is sealed. When a current is injected at $X = 0$, the expression for $\tilde{V}(x, s)$ in such a cylinder is

$$\frac{\tilde{V}(x, s)}{\tilde{V}(0, s)} = \frac{\cosh((L - X) \cdot q) + (R_\infty/(q \cdot \tilde{R}_L(s))) \cdot \sinh((L - X) \cdot q)}{\cosh(L \cdot q) + (R_\infty/(q \cdot \tilde{R}_L(s))) \cdot \sinh(L \cdot q)} \quad (23)$$

where $q = (1 + \tau \cdot s)^{1/2}$.

At the origin of this cylinder, $X = 0$, the expression for the input impedance is

$$\frac{q \cdot \tilde{R}_{in}(0, s)}{R_\infty} = \frac{1 + (R_\infty/(q \cdot \tilde{R}_L(s))) \cdot \tanh(L \cdot q)}{R_\infty/(q \cdot \tilde{R}_L(s)) + \tanh(L \cdot q)} \quad (24)$$

Equations 23–24 can be found, in different forms, in different publications (Rall, 1960; Butz and Cowan, 1974; Horwitz, 1981; Koch and Poggio, 1985; Holmes, 1986). When the input is not at the origin of the cylinder, the input admittance at the input point, y, is the sum of the various directional input admittances at point y. For example, consider the case of a point y along a finite cylinder. There are two possible directions (denoted by 1 and 2) for the signal at point y, one into cylinder 1 and the other into cylinder 2. The input admittance at point y is

$$\tilde{G}_{in}(y, s) = \vec{\tilde{G}}_{in,1}(y, s) + \vec{\tilde{G}}_{in,2}(y, s) \quad (25)$$

where $\vec{\tilde{G}}_{in,1}(y, s)$, $\vec{\tilde{G}}_{in,2}(y, s)$ are the directional input admittances to cylinders 1 and 2, respectively.

Rate of voltage attenuation in the Laplace domain

The expression for the rate of attenuation of the Laplace transform voltage at point x, defined as the absolute value of the ratio between $\partial\tilde{V}/\partial x$ and $\tilde{V}$ at this point, is

$$\left|\frac{\partial \tilde{V}(x, s)/\partial x}{\tilde{V}(x, s)}\right| = \left|\frac{\partial \ln(\tilde{V}(x, s))}{\partial x}\right| = \frac{\vec{r}_i}{\vec{\tilde{R}}_{in}(x, s)} = \frac{\vec{R}_\infty}{\vec{\tilde{R}}_{in}(x, s) \cdot \vec{\lambda}} \quad (26)$$

where the directional properties and the derivative correspond to the direction in which the signal propagates (Eq. 26 is the Laplace domain analogue of the basic expression $\partial V(x, t)/\partial x = -\vec{I}_i(x, t) \cdot \vec{r}_i$, where $\vec{I}_i(x, t) = V(x, t)/\vec{R}_{in}$ represents the intracellular current; see Rall, 1989, equation 2.5). We can see that the attenuation rate of the Laplace transform of the signal depends only on the details of the structure in "front" of the signal and is independent of the structure "behind" the signal and the input location.

COMPUTATIONAL METHODS

This work is purely theoretical. The main software tool used is Mathematica (Wolfram Research, Inc., 1993). It was used intensively for proving the theorems, developing and simplifying the mathematical expressions, implementing the algorithms, analyzing the results, and preparing the figures. It could be very hard to obtain some of the complicated expressions in this work without the use of a computerized system for algebraic manipulation of expressions. The detailed code in Mathematica format for the various computations and graphical representations can be obtained from the author. The symbolic results of Mathematica were verified by hand and by comparing to the results of numerical examples.

STRENGTH, RESISTANCE, AND ATTENUATION FOR TRANSIENT SIGNALS

In this section, the properties of the time integral (zeroth moment) of a transient signal are analyzed. Rinzel and Rall (1974) showed the similarity between the equations of the time integral of the voltage response in a passive structure (Eq. 19) and the steady-state cable equations. This similarity holds for any time-invariant linear system. Specifically, in such a system, if the zeroth moment of the transient input is A and the zeroth moment of the output response is B, then if we apply a steady input of magnitude A to that system, we get a steady output of magnitude B. This important feature of time-invariant linear systems allows one to apply the same methods used for the analysis of steady-state inputs to the analysis of the zeroth moment. Hence, we can easily prove the following theorems concerning the properties of the zeroth moment (the proofs are given in the Appendix).

Theorems

Theorem I (shape invariance)

The transfer resistance and the attenuation factor between any two given points (y, x) in a passive structure are independent of the shape of the injected transient current. As a special case, the input resistance at any point in a passive structure is independent of the shape of the injected transient current (Fig. 3 *A*).

Theorem II (reciprocity)

Given two points (y, x) in a passive structure, $R_{tr}(y, x) = R_{tr}(x, y)$. Note that this is *not* true for the attenuation factor between those points (Fig. 3 *B*).

Theorem III (attenuation rate theorem)

The attenuation rate of the voltage response signal depends only on the details of the structure in "front" of the signal. Hence, the attenuation rate is independent of the structure "behind" the signal and the current injection point (Fig. 4 *A*). One consequence of this theorem is that $A(y, x)$ does not depend on the location of the transient input, provided that it is at or behind point y.

Theorem IV (input resistance theorem)

The input resistance (and input conductance) defined with respect to the transient input (see definition above) are equal to the conventional definitions for steady-state input resistance (conductance). Hence, the input conductance at any

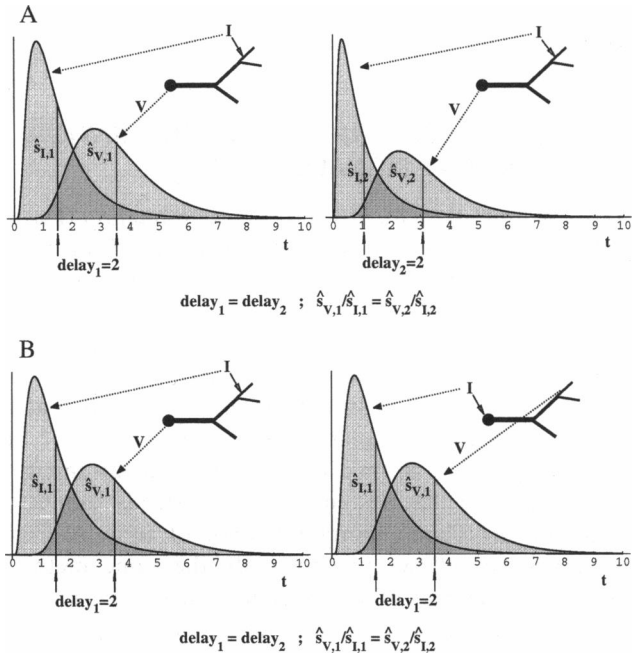

FIGURE 3 Schematic illustration of Theorems I and II for signal strength and characteristic time in passive dendritic trees. (*A*) An example of the shape invariance theorems (I). A transient current I is injected at a given point in the dendritic tree, and the voltage response V is recorded at another point. Although the injected current is different in the right and the left graphs, the transfer resistance and the transfer delay between the two points are the same. (*B*) An example of the reciprocity theorems (II). In the left graph, a transient current is injected at a given point in the dendritic tree, and the voltage response is recorded at another point. In the right graph the injecting electrode and the recording electrode interchange. The transfer resistance and the transfer delay in both graphs are the same.

point in a passive structure is the sum of the various directional input conductances at this point (Fig. 4 *B*).

Theorem V (equivalence theorem)

When analyzing input/transfer resistance and voltage attenuation in a passive structure, one can compute the input resistance and attenuation factor in any cylindrical segment, replacing the structures (subtrees) at its boundaries by the (directional) input resistance of the corresponding original structure (subtree) (Fig. 4 *C*).

Theorem VI (multi-inputs theorem)

In a passive structure, if $V_1(x, t)$ is the response to input $I_1(y_1, t)$, and if $V_2(x, t)$ is the response to input $I_2(y_2, t)$, then the strength of the response to the input $I_1 + I_2$ at point x is the sum of the strengths of V_1 and V_2 at this point.

Effective λ

For analyzing attenuation in passive trees, we define the effective space constant, $\vec{\lambda}_{eff}$, which is a generalization of the conventional space constant, λ. Its functional interpretation can be demonstrated when a steady-state current is injected at a given point. The rate of spatial voltage attenuation at this point in a given direction is inversely proportional to $\vec{\lambda}_{eff}$ in this direction. For an infinite cylinder $\vec{\lambda}_{eff} = \lambda$ at any point and in both directions. The definition of $\vec{\lambda}_{eff}$ is

$$\vec{\lambda}_{eff}(x) \equiv \left|\frac{dV/dx}{V}\right|^{-1} = \left|\frac{d\ln(V)}{dx}\right|^{-1} = \left(\frac{\vec{r}_i}{\vec{R}_{in}(x)}\right)^{-1} = \left(\frac{\vec{R}_\infty}{\vec{R}_{in}(x)\cdot\vec{\lambda}}\right)^{-1} = \frac{\vec{R}_{in}(x)}{\vec{R}_\infty}\cdot\vec{\lambda}, \quad (27)$$

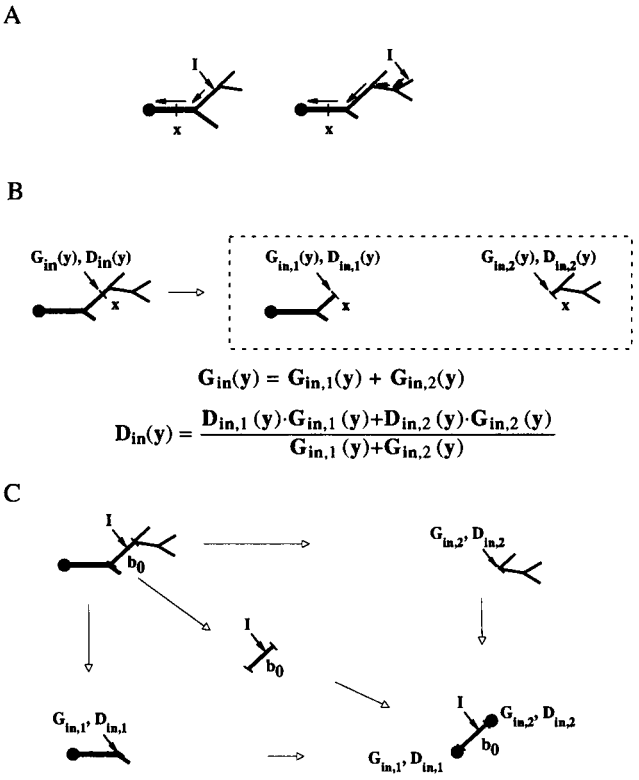

FIGURE 4 Schematic illustration of Theorems III, IV, and V for signal strength and characteristic time in passive dendritic trees. (*A*) An example of the "structural invariance" theorems (III). In the two models shown, the structure left of point x is the same. The structure to the right of point x is different, and the current injection point is different. Nevertheless, the attenuation rates and the velocities of the voltage responses that propagate to the left of point x are the same in both cases. (*B*) An example of the input resistance/conductance theorem and the input delay theorem (IV). For calculating the input conductance and the input delay at point x in the passive structure, one can split the structure at point x, calculate the input conductances and input delays at point x in the split structures, and use the given expressions to obtain the input conductance and delay at point x in the original structure. (*C*) An example of the equivalence theorems (V). The input conductance, input delay, attenuation, and propagation delay at every point along the cylinder b_0 can be computed by replacing the subtrees at the boundaries of the cylinder with simple structures (e.g., passive isopotential structures) that have the same input conductances and input delays as the original subtrees. In the figure, the input conductance, input delay, attenuation factor, and propagation delay along b_0 are the same in the upper left model and in the bottom right model.

where the directional properties and the derivative correspond to the direction to which the signal propagates (see Eq. 26).

From the analogy between the signal zeroth moment and the steady-state case, it is clear that the attenuation rate (defined with respect to the strength of a transient signal) at a given point in a given direction is equal to the corresponding rate of steady-state attenuation, and hence equal to $1/\vec{\lambda}_{eff}$ at this point in the given direction. The mathematical expression connecting the signal attenuation factor, $A(y, z)$, to the $\vec{\lambda}_{eff}$ of the points on the path between y and z is

$$\ln(A(y, z)) = \ln(V(y)) - \ln(V(z)) = \int_z^y \frac{d \ln(V)}{dx} dx = \int_y^z \frac{dx}{\vec{\lambda}_{eff}(x)}, \quad (28)$$

where $\vec{\lambda}_{eff}$ corresponds to the propagation direction. Compare this relation to the definition of generalized electrotonic distance of Rall (1962a) as $\int_y^z dx/\lambda(x)$. Equation 28 and the additivity property of integrals along a path yield a proof for the additivity property of the log attenuation factor, say, $\ln(A(y, z)) = \ln(A(y,x)) + \ln(A(x, z))$ if x is on the flow path of the current from y to z.

$\vec{\lambda}_{eff}$ may be used for obtaining a transformed representation of the structure, in which each unit of distance represents an e-fold attenuation of voltage. Obviously, this transform depends on the site of current injection (and thus the direction of current flow) in the tree. The transformation is done by scaling every infinitesimally small cylinder of length dx in the structure by $\vec{\lambda}_{eff}$ corresponding to the direction of current flow (i.e., its new length will be $dx/\vec{\lambda}_{eff}$). See Zador et al. (1995) for details and examples of use.

Calculating input resistances and attenuation factors in dendritic trees with arbitrary branching

Before analyzing dendritic trees with arbitrary branching, we should analyze the much simpler model of a cylinder that has a dendritic load, $\tilde{R}_L(s)$, at one side and a sealed end at the other side. Setting $s = 0$ (and, thus, $q = 1$) in Eqs. 23 and 24 yields equations for computing the input resistance and attenuation factor in this model. Not surprisingly, these equations are identical to the analogous equations for the steady-state case (Rall, 1989, equations 2.25 and 2.37):

$$A(0, X) = \frac{V(0)}{V(X)} = \frac{\cosh(L) + (R_\infty/R_L) \cdot \sinh(L)}{\cosh(L - X) + (R_\infty/R_L) \cdot \sinh(L - X)} \quad (29)$$

$$R_{in}(0) = R_\infty \cdot \frac{1 + (R_\infty/R_L) \cdot \tanh(L)}{R_\infty/R_L + \tanh(L)}, \quad (30)$$

where current is injected at the cylinder origin, $X = 0$, a passive dendrite is connected at the other end, $X = L$. R_L is the input resistance of the dendritic load connected to point $X = L$.

Using these equations, Rall (1959) derived recursive algorithms for computing input resistance and steady-state attenuation factor in a passive dendritic tree with arbitrary branching. These algorithms are also valid for the analysis of the strength of transient signals. The insights that were gained from the extensive analysis of the steady-state case (e.g., in Rall and Rinzel, 1973; Jack et al., 1983; Rall, 1989) are all applicable to the analysis of the strength of transients and will not be discussed further here.

DELAY

This section focuses on the properties of the centroid of the voltage response as it propagates along a dendritic tree. Several general theorems concerning delays (defined with respect to the centroid) are proved (see the Appendix). These theorems are analogous to the theorems of the signal strength. Expressions and algorithms for computing delays in passive dendrites are also derived.

Theorems

Theorem I (shape invariance)

The transfer delay and the propagation delay between any two given points (y, x) in a passive structure are independent of the shape of the injected current. As a special case, the input delay at any point in a passive structure is independent of the shape of the injected transient current (Fig. 3 *A*).

Theorem II (reciprocity)

Given two points (y, x) in a passive structure, $D_{tr}(y, x) = D_{tr}(x, y)$. Note that this is *not true* for the propagation delay between these points (Fig. 3 *B*).

Theorem III (velocity theorem)

The velocity of the voltage response signal depends only on the details of the structure in "front" of the signal. Hence, it is independent of the structure "behind" the signal and of the current injection point (Fig. 4 *A*). The consequence is that $PD(y, x)$ does not depend on the location of the input, provided that it is at, or behind, point y.

Theorem IV (input delay theorem)

The input delay at any point y in a passive structure is the weighted average of the various directional input delays at this point. The directional input delays are weighted by the corresponding directional input conductances at the point. For example, in the case of a point y along a finite cylinder, there are two possible directions (denoted by 1 and 2) for the signal at point y, one into "half"-cylinder 1 and the other

into "half"-cylinder 2. The input delay at y is

$$D_{in}(y) = \frac{\vec{D}_{in,1}(y) \cdot \vec{G}_{in,1}(y) + \vec{D}_{in,2}(y) \cdot \vec{G}_{in,2}(y)}{\vec{G}_{in,1}(y) + \vec{G}_{in,2}(y)}, \quad (31)$$

where $\vec{G}_{in,1}$, $\vec{G}_{in,2}$ are the input conductances to cylinders 1 and 2, respectively, and $\vec{D}_{in,1}$, $\vec{D}_{in,2}$ are the input delays to cylinders 1 and 2, respectively (Fig. 4 *B*).

Theorem V (equivalence theorem)

When analyzing delays in a passive structure, one can compute delays in any segment, replacing the structures (subtrees) at its boundaries by isopotential passive compartments (RC circuits), each compartment having the same (directional) input resistance and input delay as the corresponding original structure (subtree) (Fig. 4 *C*).

Theorem VI (multi-inputs theorem)

Let $V_1(x,t)$ be the response to input $I_1(y_1, t)$, and let $V_2(x, t)$ be the response to input $I_2(y_2, t)$. The characteristic time of the voltage response at point x when the input is $I_1 + I_2$ will be denoted by $\hat{t}_{V1 + V2}(x)$. This characteristic time is then

$$\hat{t}_{v_1+v_2}(x) = \frac{\hat{t}_{v_1}(x) \cdot \hat{s}_{v_1}(x) + \hat{t}_{v_2}(x) \cdot \hat{s}_{v_2}(x)}{\hat{s}_{v_1}(x) + \hat{s}_{v_2}(x)} \quad (32)$$

Effective τ

Similar to the effective λ, we define the effective time constant, $\vec{\tau}_{eff}$, which extends the functional meaning of the classical τ. Given a point y in a tree and a given direction, $\vec{\tau}_{eff}$ is defined as the directional input delay in this direction. In the case of an isopotential structure, $\vec{\tau}_{eff} = \tau$. This can be shown using Eq. 35 or directly when considering a δ-function current input. In this case, the resultant voltage decays exponentially with a time constant, τ, and the centroid of such a decay is also exactly τ. Thus, for an isopotential structure, the input delay for the δ-function input is exactly τ. Because the input delay is independent of the shape of the input current (Delay Theorem I), this result is valid for any input shape.

It is important to note that, in contrast to $\vec{\lambda}_{eff}$, the transmembrane direction is a legitimate direction for $\vec{\tau}_{eff}$. For example, when the point y is at an isopotential soma that is coupled to a cylinder, two possible directions for current flow exist when $\vec{\tau}_{eff}$ is considered: the flow through the soma membrane and the flow into the cylinder. For $\vec{\lambda}_{eff}$, however, only the latter direction is relevant.

As a consequence of the proof of the Velocity Theorem (see Eq. A13), the velocity of the signal at a given point, x, can be written as $\vec{\lambda}_{eff}(x)/\vec{\tau}_{eff}(x)$, where $\vec{\lambda}_{eff}(x)$ and $\vec{\tau}_{eff}(x)$ correspond to the direction considered. For example, in an infinite cylinder, $\vec{\tau}_{eff}(x) = \tau/2$ and $\vec{\lambda}_{eff}(x) = \lambda$ at any point. Thus the velocity is $2 \cdot \lambda/\tau$ (Agmon-Snir and Segev, 1993). In Jack et al. (1983, chapter 3), it is shown analytically that the velocity of a voltage signal is asymptotically approaching $2 \cdot \lambda/\tau$ in an infinite cylinder for various definitions of velocity (e.g., the velocity of the peak of a transient signal, the velocity of the half-amplitude point for a response to a step voltage change). This relation between the velocity and the effective parameters ($\vec{\lambda}_{eff}(x)$, $\vec{\tau}_{eff}(x)$) is important and general, and can be extended to nonlinear cases (unpublished results). The mathematical expression connecting the propagation delay, $PD(y, z)$, to the velocity and to $\vec{\lambda}_{eff}$ and $\vec{\tau}_{eff}$ of the points on the path is

$$PD(y, z) = \hat{t}_v(z) - \hat{t}_v(y) = \int_y^z \frac{d\hat{t}_v(x)}{dx} dx = \int_y^z \frac{dx}{\vec{\theta}(x)} = \int_y^z \frac{\vec{\tau}_{eff}(x) \cdot dx}{\vec{\lambda}_{eff}(x)} \quad (33)$$

where $\vec{\theta}_{eff}$, $\vec{\lambda}_{eff}$, $\vec{\tau}_{eff}$ correspond to the propagation direction (compare to Eq. 28). Equation 33 and the additivity property of integrals along a path yield a proof for the additivity property of the propagation delay, say, $PD(y, z) = PD(y, x) + PD(x, z)$ if x is on the flow path of the current from y to z.

We can use the signal velocity to obtain a transformed representation of the structure, in which each unit of distance represents a unit of propagation delay. Obviously, this transform depends on the site of current injection (and thus the direction of current flow) in the tree. The transformation is done by scaling every infinitesimally small cylinder of length dx in the structure by $\vec{\theta}$ corresponding to the direction of current flow (i.e., its new length will be $dx/\vec{\theta}$). See Zador et al. (1995) for details and examples of use.

Calculating delays in dendritic trees with arbitrary branching

Again, before analyzing dendritic trees with arbitrary branching, we will analyze the much simpler model of a cylinder that has a dendritic load, $\tilde{R}_L(s)$, at one side and a sealed end at the other side. There is a straightforward method for deriving expressions for delays in such a cylinder when current is injected at its origin, $X = 0$, and the passive dendrite is connected at the other end, $X = L$. The boundary condition at $X = L$ imposed by such a dendrite is described mathematically by $\tilde{R}_L(s)$, which is the (directional) $\tilde{R}_{in}(s)$ of the dendritic tree at the point of connection (see Properties of the Laplace Transform in Passive Structures, above). Differentiating the logarithm of both sides of Eq. 23 with respect to s and setting $s = 0$, we get an expression for the propagation delay (to be precise, we get an expression for $-PD(0,X)$; see Eq. A2 in the Appendix). The same procedure applied to both sides of Eq. 24 yields, after rearranging, an expression for the input delay at

$X = 0$. After simplification, the final expressions are

$$PD(0, X) = \left(\frac{e^{L-X} \cdot (\kappa \cdot (1 + \xi) - \xi \cdot (L - X))}{\xi \cdot (\xi \cdot e^{X-L} + e^{L-X})} + \frac{\kappa \cdot (1 + \xi) - \xi \cdot L}{\xi + e^{2L}} - \frac{\kappa \cdot (1 + \xi) - \xi \cdot (L - X/2)}{\xi}\right) \cdot \tau \quad (34)$$

$$D_{in}(0) = \left(\frac{1}{2} + 2 \cdot \frac{\kappa \cdot (1 + \xi) - \xi \cdot L}{\xi^2 \cdot e^{-2L} - e^{2L}}\right) \cdot \tau \quad (35)$$

where

$$\xi = \frac{R_L - R_\infty}{R_L + R_\infty}, \qquad \kappa = \frac{R_\infty \cdot \left(\frac{1}{2} - \frac{D_L}{\tau}\right)}{R_L + R_\infty} \quad (36)$$

τ is the time constant of the membrane of the cylinder, and R_L and D_L are the input resistance and input delay of the passive load (the dendritic tree connected to point $X = L$). A simplified useful expression for the propagation delay is easily found for the case $X = L$,

$$PD(0, L) = \left(\frac{\kappa \cdot (1 + \xi) - \xi \cdot L}{\xi + e^{2L}} - \kappa + \frac{L}{2}\right) \cdot \tau \quad (37)$$

A few special cases should be explicitly considered. In the case of a sealed end at $X = L$, we get $\xi = 1$ and $\kappa = 0$ (because $R_L \to \infty$). When point $X = L$ is voltage-clamped to 0 (usually called "killed-end" boundary condition, or, more precisely, "infinitely large soma"), $R_L = 0$ and, thus, $\xi = -1$ (κ vanishes from the expression). Also, when $\xi = 1$, $\kappa = 0$ and $L \to 0$, we get, using l'Hôpital's rule, the input delay of an isopotential passive compartment, τ.

As seen in Eqs. 34 and 35, the dendritic load can be substituted by a passive isopotential compartment characterized by R_L and D_L for the purpose of computing delays (see Equivalence Theorem for delays and Fig. 5). The total membrane resistance of this isopotential compartment is R_L, and the time constant of its membrane is D_L (as explained in the subsection on the effective τ above, D_{in} of an isopotential structure is the time constant of its membrane). Note that it is not required that the membrane time constant of the cylinder and of the segments of the dendritic tree would be the same.

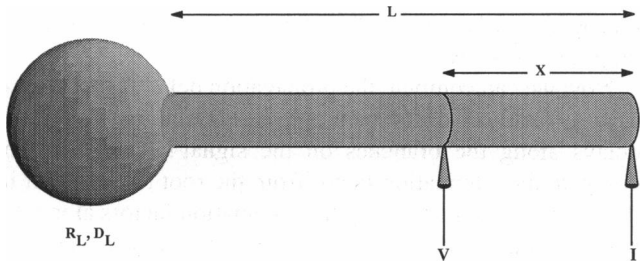

FIGURE 5 Model of Eqs. 34 and 35. A passive cylinder of electrotonic length L is connected to a passive isopotential structure. The input resistance of the isolated isopotential structure is its total membrane resistance, and its input delay is the time constant of its membrane. As explained in the text, for delay calculations, every passive dendritic load can be reduced to an isopotential structure that has the same input resistance and input delay as the original load. Equations 34 and 35 in the text refer to the model depicted here.

Using recursive substitutions of dendritic loads by isopotential structures, one can compute delays in a passive tree with arbitrary branching. The algorithms are analogous to the recursive algorithms of Rall (1959) for the steady-state case. We will describe these algorithms here: first, the algorithm for computing input delay (and input resistance) at the root of a passive dendritic tree; then, the algorithm for computing propagation delays (and attenuation factors) from the root of a passive dendritic tree; and finally, a novel algorithm that computes efficiently the input delays and input resistances at all branchpoints of the tree, as well as the propagation delays and attenuation factors along all segments (and in both directions) of the tree.

The algorithm for computing input delay (and input resistance) at the root of a passive dendritic tree is described using Fig. 6. A dendritic tree may be in the form depicted in (3), i.e., a cylinder connected to a subtree (T_1) at its far end. For computing the input resistance and input delay at the root of the full tree, we should first compute the input resistance and input delay at the root of T_1 (when T_1 is isolated). Then we can compute the input resistance and input delay at the root of the full tree, using Eqs. 30 and 35. In the graphical representation of Fig. 6, this is shown by substituting T_1 by an equivalent isopotential structure, and then using (2) to substitute the resultant "cylinder-soma" structure by another isopotential structure. Computing the input resistance and the input delay of this isopotential structure is trivial and shown in part (1) of Fig. 6.

We were left with the problem of calculating the input resistance and input delay at the root of T_1. This tree is in the form depicted in (4), i.e., two subtrees connected at their root. T_1 of (3) is now the full tree in (4), and its two subtrees are denoted T_1 and T_2. We know how to compute the input resistance and input delay at the root of these subtrees (when they are isolated from each other), because each of them is of the form (3). After computing these values, we can use the input resistance and input delay theorems (Theorems IV) to compute the equivalent input resistance and input delay at the root of the full tree (which is T_1 of the original dendritic tree).

The recursion is stopped when we get to the distal tips. At the most distal branchpoints we encounter structures of the form (4), but T_1 and T_2 are just sealed cylinders. To compute the input resistance and input delay at the root of these cylinders, we use (2) for the special sealed case, i.e., we use Eqs. 30 and 35 with $R_L \to \infty$ ($\xi = 1$ and $\kappa = 0$).

If the tree has a passive soma at its root, it can be treated as every other isopotential structure. After computing the input resistance and input delay at the root of the tree without the soma, the input resistance and input delay of the

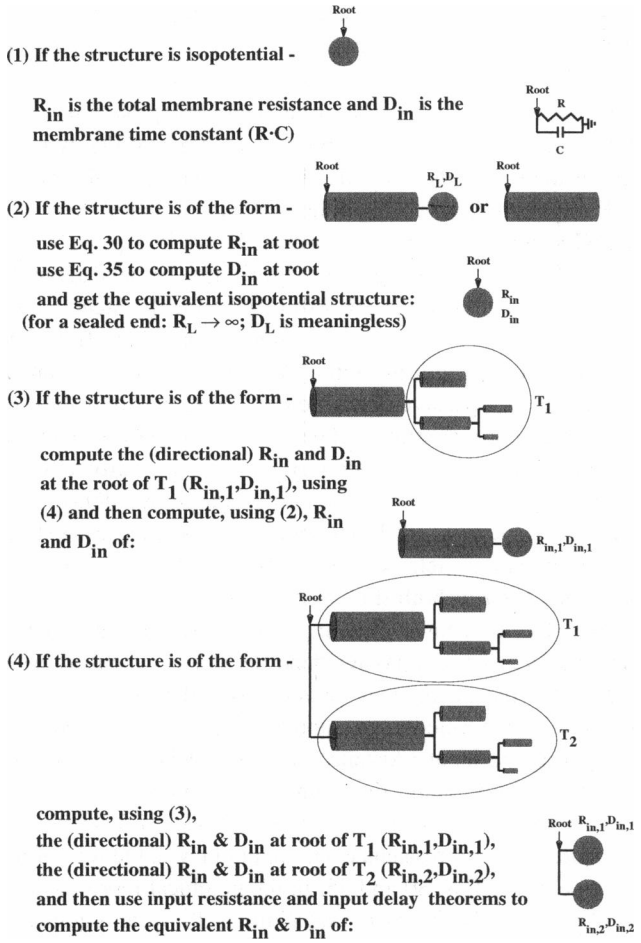

FIGURE 6 A recursive algorithm for computing R_{in} and D_{in} at the root of a passive dendritic structure. This recursive algorithm is similar to Rall's algorithm for computing R_{in} at the root of a passive dendritic structure. Its computation time scales linearly with the number of branches in the structure. Every point in a dendritic structure can be considered the root of the structure, and then the R_{in} and the D_{in} at this point can be computed.

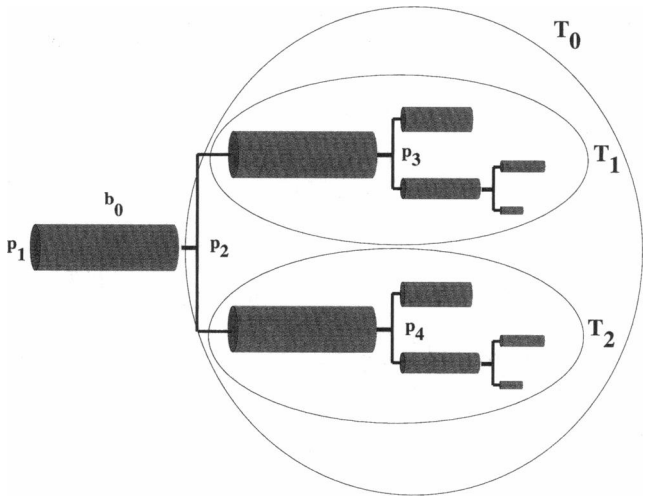

FIGURE 7 Schematic figure for the algorithms described in the text. The structure in the figure consists of a cylinder denoted by b_0 and a dendritic load denoted by T_0. T_0 consists of two subtrees, denoted T_1 and T_2. p_1 is the root of the structure; p_2, p_3, and p_4 are branchpoints. One algorithm is for calculating the propagation delays and attenuation factors along the branches for the case when an input is injected at p_1. After computing the input resistance and the input delay of T_0 (using the algorithm described in Fig. 6), the propagation delay along b_0 can be calculated. In the same way, the propagation delay along the branches in T_1 and T_2 can be calculated. Another algorithm, described in text, is used for calculating the propagation delays and attenuation factors for a signal that propagates proximally, and for calculating the input resistance and input delay at every branchpoint in the structure. The computation time of these algorithms scales linearly with the number of branches in the structure.

whole tree (with the soma) are computed using Theorems IV. This is a special case of form (4).

The second algorithm computes propagation delays (and attenuation factors) from the root of a passive dendritic tree. This algorithm consists of two steps:

1. Computing R_{in} and D_{in} at the root of the structure, using the algorithm just described. The important addition is that we keep the values of $\vec{R}_{in}$ and $\vec{D}_{in}$ found at the roots of all the subtrees in the structure. In other words, if our tree is of form (3) of Fig. 6, we compute the input resistance and input delay at the root of T_1 and save these values. Also, we keep the values computed for T_1 and T_2 for trees of the form (4). After this stage, we have, for each branchpoint, the input resistance and the input delay of the trees distal to this point.

2. Computing attenuation factors and propagation delays along the branches of the dendritic tree for a signal that propagates distally. Fig. 7 shows a sample dendritic tree, and we assume an input at its root, p_1. The root branch b_0 is connected to a dendritic load T_0. We know (from the previous step) the input resistance and the input delay at the root of the isolated T_0. Hence, we can compute the attenuation factor along b_0 using Eq. 29 and the propagation delay using Eq. 34 (or Eq. 37 for the overall propagation delay along the branch). We continue recursively to subtrees T_1 and T_2, calculating the attenuation factor and propagation delay along their root branches. (Eqs. 29, 34, and 37 are applicable here, although these branches are not sealed at one end. This is a result of Theorems III (attenuation-rate and velocity.) At the end of the full recursive process, we have the attenuation factor and propagation delay along all of the branches for a signal that propagates distally.

Now we can compute the propagation delay from the root to any point in the structure by adding the propagation delays along the branches on the signal's path. We can compute the attenuation factor from the root to any point in the structure by multiplying the attenuation factors along the branches on the signal's path. Moreover, as a trivial outcome of Theorems III, one can compute the propagation delay and attenuation factor from every point to every point that is distal to it by adding propagation delays along the path and by multiplying attenuation factors along it.

In fact, for every branch in the tree, there are just two possible values for the propagation delay between its ends. One is for the case of a signal propagating toward one end,

and the other for the case of a signal propagating toward the other end. The location of the input (provided that it is not inside the branch—in this case we should split the branch at the input site) is not important. It is only important to know if the input is in the structure connected to one end of the branch or in the structure connected to the other end of it. This is another outcome of Theorems III. The same argument holds for the attenuation factor along a branch.

This leads us to the third algorithm, which computes the input resistance and input delay at every branchpoint, as well as the propagation delays and attenuation factors along all segments (and to both directions) of the tree. The first algorithm described above allows us to find, for each branchpoint, the input resistance and the input delay of the trees distal to this point. In other words, we find, for each branchpoint, the directional input resistances and input delays at this point to the distal directions. However, the values of the directional input resistances and input delays to the proximal direction are still not known. These missing values can be found using another recursive algorithm.

To see that, we go back to Fig. 7. For the root, p_1, there is no proximal direction, so all of the directional values (of input resistance and input delay) are known. When we continue to p_2, we see that we already have the directional values at this point in the direction of T_1 and in the direction of T_2. The proximal direction is easy to compute, as the structure to this direction is just a cylinder of the form (2) of Fig. 6 (and, hence Eqs. 30 and 35 should be used with $R_L \to \infty$).

Having all of the directional values at p_2, we can continue to points p_3 and p_4. For these points, the distal directional values were computed before. It is not hard to compute the directional values in the proximal direction of p_3. The structure in this direction is a cylinder with a dendritic load. We can calculate the input resistance and the input delay of this dendritic load, as we know all of the directional input resistances and the input delays at p_2 (we only need the directional values at p_2 in the proximal direction and in the direction of T_2; then we use Theorems IV to get the input resistance and the input delay of this dendritic load). The same process can be applied to p_4, and we can continue recursively to distal points at the tree.

After completing this step, we know the directional input resistances and input delays in all directions at every branchpoint and, hence, we can compute the dendritic load at both sides of each branch. Therefore, using Eqs. 29 and 34 (or Eq. 37), we can compute for every branch the attenuation factors and propagation delays along it to both directions (in fact, the proximal directional values and the attenuation factors and propagation delays can be computed at the same pass over the tree).

The computation time of all of the above algorithms scales linearly with the number of the branches in the structure (and is independent of the length of the branches). After the calculations of the last algorithm, the attenuation factor and propagation delay between any two points in the tree can be easily found. Because the input resistance and input delay are computed for all branchpoints, the transfer resistance and transfer delay can also be found between any two branchpoints.

The expressions and algorithms described in this section may be extended to more general passive trees, including spiny dendrites (e.g., by modeling a spine as a cylinder connected to an isopotential compartment at one end and to the dendrite at the other end), tapering cables (e.g., by developing alternative expressions from the solution to the relevant cable equation), etc. Many important insights can be gained from analysis of dendritic delays using the theorems, expressions, and algorithms above. A detailed analysis of delays and time windows for input synchronization in dendritic trees, using the above results, is given in Agmon-Snir and Segev (1993) and Agmon-Snir (1994). See also Discussion below.

BROADENING

In this section, we discuss the properties of the signal width and broadening as the signal propagates along dendritic trees. The analysis is similar to the preceding analysis of attenuation and delay, with corresponding definitions, theorems, and algorithms.

For analyzing broadening, we introduce the broadening parameter, η, defined for any given point in a tree as $\eta = B_{in} - (D_{in})^2$. We will also use $\vec{\eta}$, defined as $\vec{\eta} = \vec{B}_{in} - (\vec{D}_{in})^2 = \vec{B}_{in} - (\vec{\tau}_{eff})^2$ for a given point and a direction. It is easy to analyze the isopotential structure model and show that η is 0 in this case. For the non-isopotential case, $\eta > 0$. The broadening parameter is used in Broadening Theorems III and IV below.

Theorems

See the Appendix for proofs of the following theorems.

Theorem I (shape invariance)

The transfer broadening and the propagation broadening between any two given points (y, x) in a passive structure are independent of the shape of the injected current. In particular, the input broadening at any point in a passive structure is independent of the shape of the injected current.

Theorem II (reciprocity)

Given two points (y, x) in a passive structure, $B_{tr}(y, x) = B_{tr}(x, y)$. Note that this is not true for the propagation broadening between these points.

Theorem III (broadening rate theorem)

The broadening rate of the voltage response signal depends only on the details of the structure in "front" of the signal. Hence, it is independent of the structure "behind" the signal and of the current injection point. The consequence is that $PB(y, x)$ does not depend on the location of the input (provided that it is at or behind point y). The

broadening rate of the signal at a given point, x, is given by $\vec{\eta}(x)/\vec{\lambda}_{eff}(x)$, where $\vec{\lambda}_{eff}(x)$ and $\vec{\eta}(x)$ correspond to the direction considered.

As in Eq. 33, the relation between the propagation broadening, the broadening rate, and $\vec{\eta}$ can be easily expressed. Then, the additivity property of the propagation broadening may be easily proved, say, $PB(y, z) = PB(y, x) + PB(x, z)$, if x is on the flow path of the current from y to z.

Theorem IV (input broadening theorem)

η at any point y in the passive structure is the weighted average of the various $\vec{\eta}$ to the possible directions from y. The weighting is by the corresponding directional input conductances. For example, in the case of a point y along a finite cylinder, there are two possible directions (denoted by 1 and 2) for the signal at point y, one into "half"-cylinder 1 and the other into "half"-cylinder 2. η at y is

$$\eta(y) = \frac{\vec{\eta}_1(y) \cdot \vec{G}_{in,1}(y) + \vec{\eta}_2(y) \cdot \vec{G}_{in,2}(y)}{\vec{G}_{in,1}(y) + \vec{G}_{in,2}(y)} \tag{38}$$

where $\vec{G}_{in,1}$, $\vec{G}_{in,2}$ are the input conductances to cylinders 1 and 2, respectively, and $\vec{\eta}_1$, $\vec{\eta}_2$ are the directional η to cylinders 1 and 2, respectively. The input broadening can then be computed by $B_{in} = \eta + (D_{in})^2$.

Theorem V (equivalence theorem)

When analyzing broadening in a passive structure, one can compute the broadening in any segment, representing each structure (subtree) at the segment boundaries by the (directional) input resistance, input delay, and input broadening of the corresponding structure (subtree).

Theorem VI (multi-inputs theorem)

Let $V_1(x, t)$ be the response to input $I_1(y_1, t)$, and let $V_2(x, t)$ be the response to input $I_2(y_2, t)$. The symbol for the dispersion of the voltage response at point x, as a response to the input $I_1 + I_2$, will be $\hat{w}^2_{V1 + V2}(x)$. This dispersion is then

$$\hat{w}^2_{v_1+v_2}(x) = \frac{(\hat{w}^2_{v_1}(x) + \hat{t}^2_{v_1}(x)) \cdot \hat{s}_{v_1}(x) + (\hat{w}^2_{v_2}(x) + \hat{t}^2_{v_2}(x)) \cdot \hat{s}_{v_2}(x)}{\hat{s}_{v_1}(x) + \hat{s}_{v_2}(x)} - (\hat{t}_{v_1+v_2}(x))^2 \tag{39}$$

Calculating broadening in dendritic trees with arbitrary branching

Starting with the simple model of a cylinder that has a dendritic load, $\tilde{R}_L(s)$, at one side and a sealed end at the other, we can use a straightforward procedure for deriving expressions for broadening in this cylinder. The current is injected at the cylinder origin, $X = 0$, and the passive dendrite is connected at the other end, $X = L$. Differentiating twice the logarithm of both sides of Eq. 23 with respect to s and setting $s = 0$, we get an expression for the propagation broadening. The same procedure applied to Eq. 24 yields, after rearranging, the input broadening at $X = 0$. The final simplified (and yet complicated) expressions are

$$B_{in}(0) = \frac{\tau^2}{2} + \left(\frac{4 \cdot e^{2L} \cdot \xi \cdot (\kappa + \kappa \cdot \xi - \xi \cdot L)^2}{(\xi^2 - e^{4L})^2}\right) \cdot \tau^2 + \left(\frac{e^{2L}(\alpha \cdot (\xi^2 - \xi^3 + \xi - 1) + 8 \cdot \kappa \cdot L + \xi \cdot (8 \cdot \kappa^2 - 2 \cdot L - 4 \cdot L^2) + \xi^2 \cdot (8 \cdot \kappa^2 + 2 \cdot L - 8 \cdot \kappa \cdot L + 4 \cdot L^2))}{2 \cdot (\xi - 1) \cdot (e^{2L} - \xi) \cdot (e^{2L} + \xi)}\right) \cdot \tau^2 \tag{40}$$

$$PB(0, X) = \frac{\tau^2}{4 \cdot (1 - \xi) \cdot (e^{2L} + \xi)^2 \cdot (e^{2L} + e^{2X} \cdot \xi)^2} \cdot \{4 \cdot \kappa^2 \cdot e^{2L} \cdot (e^{2L} \cdot ((\xi^3 + 1) \cdot (1 - e^{4X}) + \xi \cdot (1 + \xi) \cdot (1 + 2 \cdot e^{2L} \cdot (1 - e^{2X}) - e^{4X})) + 2 \cdot \xi \cdot (1 + \xi) \cdot e^{2X} \cdot (1 - e^{2X})) + e^{2L} \cdot (e^{2X} - 1) \cdot (\xi - 1) \cdot [(\alpha \cdot (e^{2L} \cdot \xi^2 - \xi - e^{2L} + \xi^3) - 2 \cdot L \cdot \xi \cdot (e^{2L} + \xi)) \cdot (e^{2L} + e^{2X} \cdot \xi) + 4 \cdot e^{4L} \cdot (2 \cdot \kappa \cdot L + 2 \cdot \kappa \cdot \xi \cdot L - \xi \cdot L^2) + 4 \cdot e^{2X} \cdot L \cdot \xi^2 \cdot (\xi \cdot L - 2 \cdot \kappa \cdot (\xi + 1))] + X \cdot (e^{2L} + \xi)^2 \cdot (\xi - 1) \cdot (4 \cdot e^{2L+2X} \cdot (2 \cdot \xi \cdot L - \xi \cdot X - 2 \cdot \xi \cdot \kappa - 2 \cdot \kappa) + e^{4X} \cdot \xi^2 - e^{4L})\} \tag{41}$$

where ξ and κ are defined in Eq. 36, and

$$\alpha = \frac{2 \cdot B_L}{\tau^2} - 1 \tag{42}$$

τ is the time constant of the membrane of the cylinder, R_L, D_L, and B_L are the input resistance, input delay, and input broadening of the passive load (the dendritic tree connected to point $X = L$). These complicated expressions can be obtained from the author in electronic form (in C program-

ming language format, Fortran format, Tex format, and in Mathematica format).

A simplified useful expression for the propagation broadening is easily found for the case $X = L$,

$$PB(0, L) = \frac{\tau^2}{4 \cdot (1 - \xi) \cdot (e^{2L} + \xi)^2 \cdot e^{4L}(1 + \xi)^2} \cdot \{4 \cdot \kappa^2 \cdot (1 + \xi) \cdot (e^{4L} - 1) + \alpha \cdot (1 - e^{2L}) \cdot (\xi - 1)^2 \cdot (e^{2L} + \xi) + 8 \cdot \kappa \cdot e^{2L} \cdot (\xi^2 - 1) \cdot L + L \cdot (\xi - 1) \cdot (e^{4L} - \xi^2 - 4 \cdot L \cdot e^{2L} \cdot \xi)\} \quad (43)$$

A few special cases should be explicitly considered. In the case of a sealed end at $X = L$, we get $\xi = 1$ and $\kappa = 0$ (because $R_L \to \infty$). The appropriate expressions may be obtained by finding the limit of Eqs. 40–41 when ξ approaches 1, using l'Hôpital's rule:

$$B_{in}(0) = \frac{\tau^2}{2} + \left(\frac{4 \cdot e^{2L} \cdot L^2}{(1 - e^{4L})^2}\right) \cdot \tau^2 + \left(\frac{(1 + 2 \cdot L) \cdot e^{2L} \cdot L}{e^{4L} - 1}\right) \cdot \tau^2 \quad (44)$$

$$PB(0, X) = \frac{\tau^2 \cdot \{2 \cdot e^{2L} \cdot L \cdot (1 + e^{2L} - 2 \cdot L) - e^{2L} \cdot X \cdot (2 + e^{2L}) - X\}}{4 \cdot (e^{2L} + 1)^2} + \frac{\tau^2 \cdot e^{2L} \cdot (X - L) \cdot \{(e^{2L} + e^{2X}) \cdot (1 - 2 \cdot L + 2 \cdot X) - 2 \cdot e^{2L} \cdot (X - L)\}}{2 \cdot (e^{2L} + e^{2X})^2} \quad (45)$$

and α vanishes from the expressions. When point $X = L$ is voltage-clamped to 0, $R_L = 0$ and, thus, $\xi = -1$ (κ and α vanish from the expressions). Also, when $\xi = 1$, $\kappa = 0$ and $L \to 0$, we get, using l'Hôpital's rule, the input broadening of an isopotential passive compartment, τ^2.

As can be seen (and as was proved in Broadening Theorem V), for the analysis of broadening, the dendritic load is characterized by its input resistance, input delay, and input broadening. The algorithms described in the Delay section can be easily extended to the analysis of the signal's width and dispersion in a passive tree with arbitrary branching. These algorithms yield attenuation, delay, and broadening in a computation time that scales linearly with the number of branches in the modeled dendritic tree.

These theorems, expressions, and algorithms can yield interesting insights for the broadening of transient signals in simple and complicated structures (Agmon-Snir, 1994, and the Discussion below).

DISCUSSION

The approach suggested in this paper is based on characterizing dendritic transients by their moments-based properties. Based on the signal's strength, characteristic time, and width, the concepts of attenuation, delay, and broadening of the transient signal were defined.

Theorems about the behavior of moments-based properties are based on the close correspondence between the Laplace transform and the moments. This correspondence also yields expressions and efficient algorithms for computing the attenuation, delay, and broadening in complex trees with arbitrary branching. As a by-product, the classical definitions of the space constant (λ) and the membrane time constant (τ) are generalized. These effective λ and τ are found to be correlated to the voltage attenuation and velocity in the dendritic structure.

The moments-based properties compared to other characteristics of transient signals

Rather than using the classical measures such as the peak time (time to peak or rise time), half-width, etc. (Rall, 1967; Jack et al., 1983), we utilized here the moments-based properties of the transient signal. How do these new definitions compare to the classical ones, and under what conditions is one set of definitions more appropriate than the other?

Classically, the peak value of the potential at the target point (usually, the soma) is used as a measure for the efficacy of the excitatory postsynaptic potential (EPSP). Intuitively, this is a reasonable measure for the contribution of the EPSP to the probability of reaching threshold for spike firing. However, several investigators have noted that the time-integral of the transient signal is, in some cases, a more meaningful measure for synaptic efficacy (Jack et al., 1983; Stratford et al., 1989; Nicoll et al., 1993; Carnevale and Johnston, 1982). In practice, however, the time integral (which we call in the present work the signal strength) is mostly neglected, and the peak value retains its place as the measure of synaptic efficacy. One reason is that it is easy to read from electrophysiological recordings. Another is that it reflects the notion that an EPSP with a larger peak contributes more to the probability of spike firing than an EPSP with a smaller peak. However, the time integral of the EPSP is also an important determinant of this probability. When two EPSPs have the same peak value but have different time courses, the influence of the broader EPSP on the probability of firing is expected to be larger. Indeed, it can be shown

that in an "integrate and fire" model, where many inputs are required to reach firing threshold (Stevens, 1994), and when the inputs are not synchronized, this influence is almost proportional to the signal area rather than to the peak value. In general, for well-synchronized EPSPs that occur at the same time, the peak amplitude of the EPSPs is a more useful measure, because a voltage threshold may be reached and a spike initiated at the peak time point. For more desynchronized inputs, the time integral is expected to be more useful, because if an action potential were to be initiated, it may happen at any time point. Roughly speaking, we can say that the EPSPs occur at the same time if they arrive in a time window that is narrower than the widths of these EPSPs (see discussion about synchrony below). For more realistic models, the dependence of the firing probability on the somatic voltage is more complicated, and a combination of measures is required to predict the influence of a single PSP on this probability (see, for example, Kirkwood, 1979).

The centroid is another new measure that was introduced to define the characteristic time of the signal (it is also used in the analysis of RC networks; see Elmore, 1948; Rubinstein et al., 1983; Lin and Mead, 1984; Wyatt, 1985). Classically, the peak time is taken to be the characteristic time of the signal. In this paper, delay is defined as the difference between two centroids (rather than between the peak time of the signals). For example, the transfer delay is defined as the difference between the centroid of the current input and the centroid of the voltage response rather than the difference between the corresponding peaks. The critical difference between these two measures for the transfer delay is that, when centroids are used, the delay is independent of the input shape, whereas when the peaks are used, the delay between two given points in the tree depends on the input. Hence, the delay defined by using centroids is a robust measure that depends only on the properties of the dendritic tree.

Still, in many cases, it is interesting to measure the delay from the rising phase of the voltage response at the input point (e.g., in terms of the peak time) to the rising phase of the somatic response. This delay may be approximated by using centroids. It can be shown that this delay, measured between the PSP at some dendritic location, d, and the resultant PSP at the soma, s, can be estimated by the propagation delay from the soma to the input point ($PD(s, d)$), defined using the centroids. To see this, note that $PD(s, d) = D_{tr}(s, d) - D_{in}(s)$ (see Definitions). Using the Reciprocity Theorem for delays, we find that $PD(s, d) = D_{tr}(d,s) - D_{in}(s)$. The decay phase of the voltage response at s, when the input is at s, is very similar to the decay phase of the response at s, when the input is at d. This is because this decay is determined mainly by τ_0 (the system time constant; see Rall, 1969; Rall et al., 1992). Hence, $D_{tr}(d, s) - D_{in}(s)$ (and thus, $PD(s, d)$) is determined mostly by the difference between the rising phases (and, thus, the peak time) of these two signals. In Agmon-Snir and Segev (1993), the $PD(s, d)$ is called the net dendritic delay and is discussed more fully.

For completeness we should note that $PD(s, d)$ is also the delay between the centroid of the input current injection at point d and the centroid of the current that reaches the soma when the soma is voltage-clamped. To see that, let us assume that without the presence of a voltage clamp, a synaptic current of $I_d(t)$ at a given point, d, would result in a somatic voltage response of $V_s(t)$ and the current that reaches the soma is $I_s(t)$. In voltage clamp conditions, the electrode at the soma would inject a current of $-I_s(t)$ to prevent a change in the somatic voltage. Mathematically, we have in this case two inputs, one at d and one at s, and the sum of their voltage responses at the soma is 0. The difference between the centroid of $V_s(t)$ and the centroid of $I_s(t)$ is $D_{in}(s)$. The difference between the centroid of $V_s(t)$ and the centroid of $I_d(t)$ is $D_{tr}(d, s) = D_{tr}(s, d)$ (reciprocity theorem). Hence, $PD(s, d)$ is also the difference between the centroid of $I_s(t)$ and the centroid of $I_d(t)$.

The signal width is the third measure discussed in the present study. Using the first three moments, a formal definition for the width was introduced. As with the classical measure of the half-width (Rall, 1967), the new measure can be interpreted as the time window for input integration at a target site (e.g., the soma). The advantage of the width defined using the moments is that it can be analyzed analytically for arbitrary structures.

It is important to emphasize that most of the insights regarding the behavior of the width are already provided by analyzing the input delay, D_{in}, which utilizes only the first two moments. It can be shown (Agmon-Snir, 1994, and see example below) that, for brief inputs, D_{in} is a good measure for the signal width at the input site (and D_{tr} is a good measure for its width at the output location, e.g., the soma). The reason is that for brief inputs, D_{in} is mostly determined by the decay phase of voltage transient (e.g., D_{in} is exactly τ for the isopotential case). Therefore, the decay rate is a reasonable measure for the width of the signal, and this width can be interpreted as the time window in which the signal affects the target point. Indeed, D_{in} could be viewed as a measure for input synchrony. In order for many inputs to summate with each other locally, they should be highly synchronized at dendritic regions with small D_{in} (implementing coincidence detection). At regions with larger D_{in}, more temporal dispersion of the inputs is permitted, and integration of the inputs is implemented (see Fig. 8). The use of delay as a measure of time window is discussed in Agmon-Snir and Segev (1993) and in Agmon-Snir (1994). Finally, we note that D_{in} (and D_{tr}) is an inappropriate estimate for the signal width when the time course of the current input is long compared to D_{in} (and D_{tr}). In this case, the width of the voltage response is determined by the width of the current input and not by the properties of the tree (Agmon-Snir, 1994, and see example below).

Because the moments-based properties of the signal are computed using the whole transient (all points), these measures are less sensitive to noise compared with the classical measures (e.g., the peak value and the peak time rely on

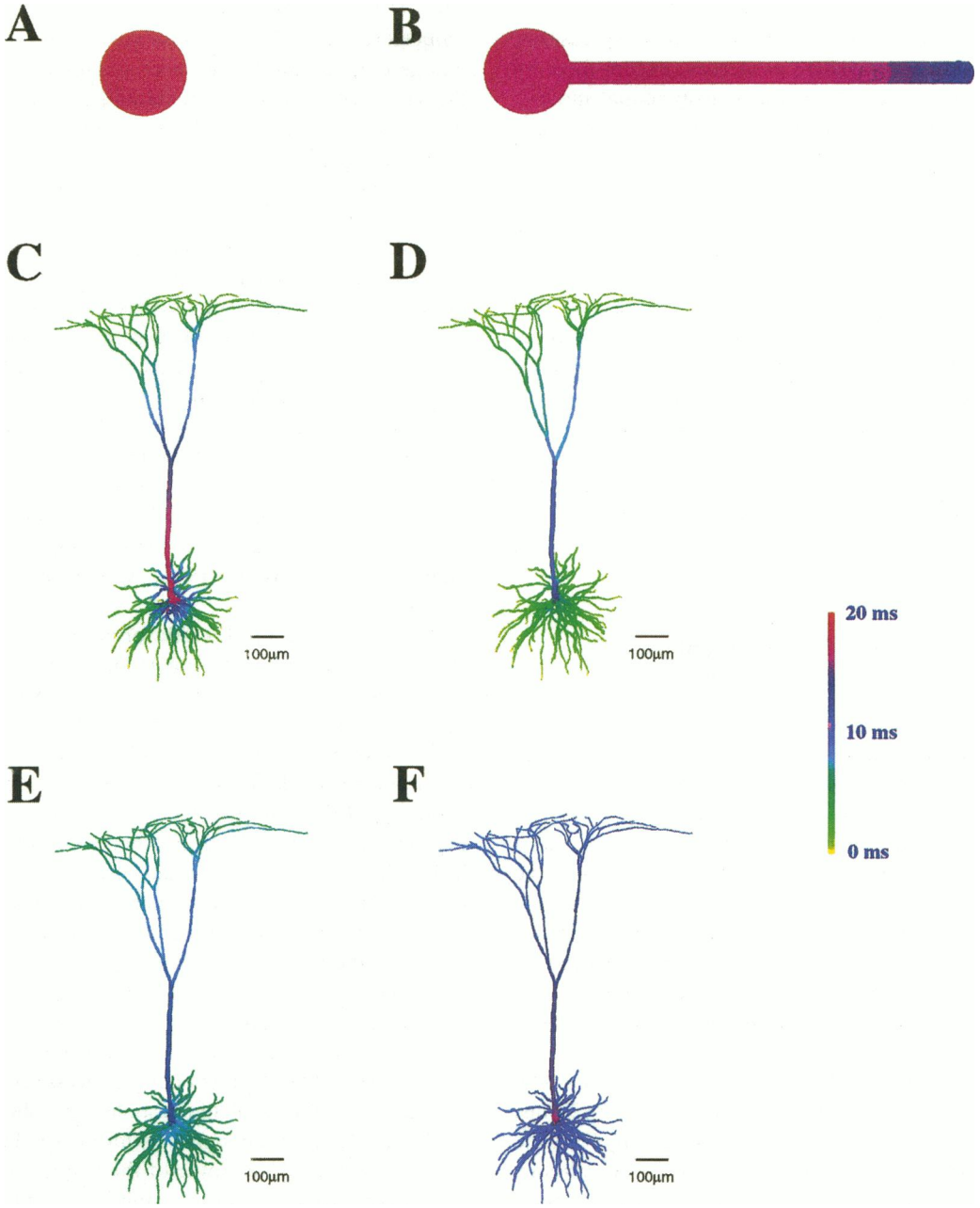

FIGURE 8 Input delay and local width in various structures. The input delay and the local width (see Discussion for definition) at every point in various structures are shown using the color code at right. In all models, the membrane time constant is 20 ms. (*A*) The input delay in an isopotential structure is the time constant of the membrane. This is also the local width for an instantaneous input. (*B*) A model of a cylinder coupled to a relatively large soma ($L = 1$, $\rho_\infty = 2.7$, $\epsilon = 1$). D_{in} at the soma is smaller than τ, the time constant of the membrane. At proximal points, D_{in} is close to τ; at distal points, D_{in} is smaller (in the case shown, it is about $\tau/2$). This is because of the electrical sink imposed by the soma. (*C*) Input delays in a reconstructed pyramidal cell from layer V in the cat visual cortex (data were kindly provided by R. Douglas). In a branched tree, the input delay at the tips can be much smaller than the membrane time constant. In the figure, the input delay at the soma is 18 ms, and at the tips the input delay is on the order of 3 ms. The calculation in the reconstructed tree was done using the recursive algorithms introduced in this article. Parameters used: $R_m = 20$ kΩ·cm^2, $R_i = 100$ Ω·cm, $C_m = 1$ μF/cm^2. Because the realistic parameters of pyramidal cells are still not known, the figure is just a demonstration of the D_{in} reduction at distal tips in branched trees, using the method of moments. (*D*) Local widths in the same model, for an instantaneous input (width = 0). (*E*) Local widths in the same model, for an input of width of 5 ms ($\tau/4$). (*F*) Local widths in the same model, for an input of width of 10 ms ($\tau/2$).

only one point). On the other hand, the moments-based properties are sensitive to the details of the transient. Using elementary electrophysiological equipment, it is much easier to measure the classical properties, but with the sophisticated data acquisition and analysis programs available today, computing the moments-based properties of synaptic potentials is rather straightforward. Another important reason for utilizing the moments-based properties is that they

provide a comprehensive and general view of dendritic transients. There is no way to state theorems, expressions, and algorithms for the classical properties, except for very simple models (e.g., infinite cylinder, isopotential model). The most important theorems in this context are the Shape Invariance Theorems that allow us to state general, shape-independent results concerning the spread of transients in passive trees.

To conclude this section we should stress that there is no single good measure for efficacy, delay, or width for all types of inputs and dendritic geometries. It is easy to find transients for which the signal strength, characteristic time, and width do not have a meaningful interpretation. Biphasic signals and signals with multiple peaks are examples of such cases. However, the classical measures also fail in most of these cases. If the moments-based properties are used, analysis can be made for the "atypical" signals by decomposing them to several "normal," monophasic signals and utilizing the Multi-inputs Theorems (Theorems VI).

Requirements for input synchronization in reconstructed dendrites: an example

In this section, we briefly demonstrate the use of the method of moments in the analysis of input synchronization in dendritic trees. For this analysis, the input delay is computed at any point in the modeled structure, using the algorithm described in Results. This input delay is used as a measure for synchrony (see above). We also compute the local width—the width of the voltage response, as defined using moments, at the point of injection. This width depends also on the width of the input. Comparing the local width of various points in the dendritic tree for a given input width may serve as a way for comparing the synchronization requirements at these points.

Fig. 8 shows the input delay and the local width in a few models; in all cases the membrane time constant is 20 ms. In the reference case of an isopotential system (Fig. 8 *A*), the input current can discharge only through the membrane. Indeed, the input delay reflects the properties of the membrane and is exactly the membrane time constant, τ. For an instantaneous input (width = 0), the local width is also τ. The isopotential reference case gives an upper limit for the input delay in passive dendritic trees because in distributed (non-isopotential) systems the input current can flow longitudinally to other regions of the tree as well as through the local membrane. Therefore, a more rapid discharge of the input current is expected, with the result of a reduced input delay associated with a briefer voltage response at the input site (Rall 1967, 1969; Rinzel and Rall 1974). This is also true for the local width for an instantaneous input. In Fig. 8 *B*, the input delay in the case of a soma coupled to a finite cylinder with a sealed end is demonstrated. Because of the conductance load (sink) imposed by the cylinder plus the soma, the input delay at distal points is reduced, compared to an isolated soma. When a complicated tree is modeled (Fig. 8 *C*) the input delay at distal sites is significantly reduced (to 0.1τ–0.2τ) because the rest of the tree serves as a large current sink for these sites. This is demonstrated by the green color in distal basal and apical tips, where the input delay is about 3 ms (compared to 18 ms at the soma). At the head of a dendritic spine, the input delay may be further reduced to 0.05τ or less (it can be shown by numerical simulations that the input delay at distal points is an overestimate of the integration time window, i.e., the time window can be much smaller; see Softky, 1994). More proximal dendritic locations may undergo very different input delays, on the order of τ (as in an isopotential model). These results were also verified by a compartmental model of the same pyramidal cell, using α-shaped input currents. We conclude that, as a general rule, input delay at distal dendritic arbors decreases as the complexity of the tree increases (this complexity can be quantified by asymmetry indices; see Nitzan et al., 1990) and that dendritic trees operate on multiple time windows for input integration (see Agmon-Snir and Segev, 1993; Agmon-Snir, 1994; Softky, 1994).

In Fig. 8 *D*, the local width for an instantaneous input is shown at every point in the reconstructed tree using the same color code. We see that the analysis of width agrees with the results of the delay analysis. Although the numbers are different, the same insights regarding synchronization requirements are demonstrated. When the input is wider, the geometry of the dendritic tree is less important in determining the synchronization requirements. This is demonstrated in Fig. 8, *E* and *F*. For an input of width of 5 ms ($\tau/4$), the local widths are still very similar to the instantaneous input case, but for an input of width of 10 ms ($\tau/2$), the input widths in the tree are on the same order of magnitude. For wider inputs, the input widths in the tree are almost the same at every point, reflecting the fact that the geometry of the tree becomes less important. We can see by comparing Fig. 8, *C* and *D–F*, that the input delay analysis may yield results regarding the width of the response for short inputs. See further analysis of the signal width in Agmon-Snir (1994).

Fig. 9 demonstrates some of the results above, showing the voltage waveforms for a sample current input injected into the same dendritic tree model used in Fig. 8. The current input is injected at time t_s and its form is $i(t) = i_{max} \cdot \alpha \cdot (t - t_s) \cdot e^{1-\alpha(t-t_s)}$, for $t \geq t_s$. In our example, $\alpha = 1\ ms^{-1}$, $t_s = 1$ ms, and i_{max} is the peak value of the current. The characteristic time of this current input is 3 ms, and its width is ($\sqrt{2}$) ms. In Fig. 9 *a*, the normalized waveforms at the injection point are shown for inputs injected at three points: at the soma, at the rightmost tip of the apical tree, and at one of the basal tips. The differences between the widths of the waveforms are as expected from the results of Fig. 8, *C* and *D*. Calculation of the input delays and input widths from the waveforms (integrated until t = 120 ms) gives results very similar to those found by the method of moments. In Fig. 9 *b*, the current is injected at the rightmost tip of the apical tree, and the normalized voltage waveforms at the injection point, at the soma, and at one of

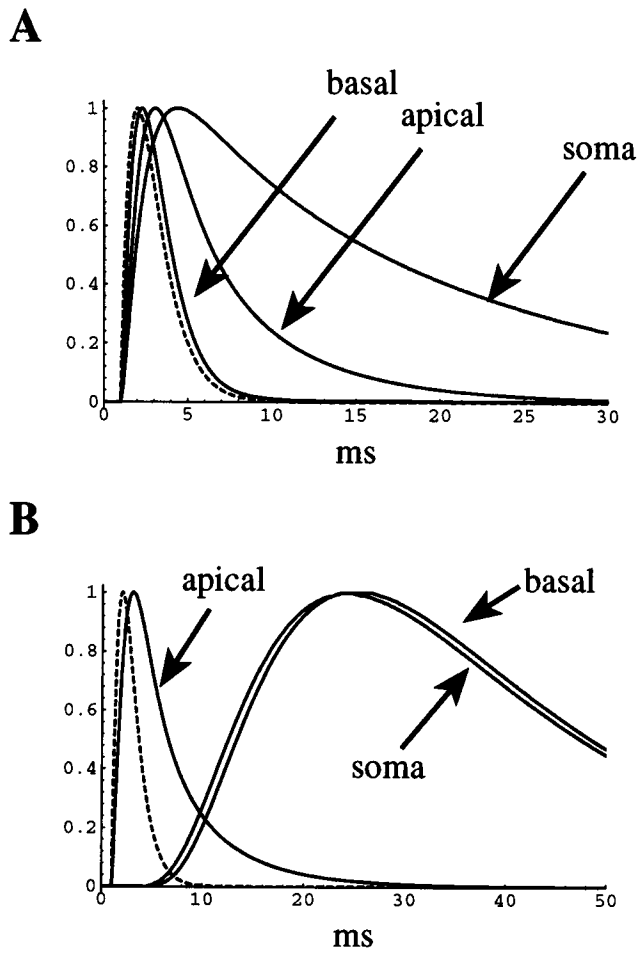

FIGURE 9 Demonstration of the method of moments results using compartmental modeling. The voltage waveforms are shown for a sample input injected to the same model used in Fig. 8. The current injected is $i(t) = i_{max} \cdot \alpha \cdot (t - t_s) \cdot e^{1-\alpha(t-t_s)}$, for $t \geq t_s$, where $\alpha = 1\ ms^{-1}$, $t_s = 1$ ms, and i_{max} is the peak value of the current. (*A*) The current is injected at a point in the tree and the local voltage response is shown. Three points were chosen: the soma, the rightmost tip of the apical tree, and one of the basal tips. The voltage responses were normalized to have the same peak value. The injected current is also shown (*dashed line*). (*B*) The current is injected at the rightmost tip of the apical tree, and the normalized voltage responses at this point, at the soma, and at one of the basal tips are shown. The injected current is also shown (*dashed line*). The simulations were done by Moshe Rapp using Neuron (Hines, 1989).

the basal tips are shown. As explained above, the delay caused by the slow-rising phase of the PSP at the soma (classically estimated by the time to peak, the rise time, and the latency) can be estimated by the propagation delay from the soma to the input point, defined using the centroids. Indeed, this PD is found to be 16.2 ms, which is a fair estimate of the delay caused by the rising phase.

An example of calculations in a simple model

An important result of the present study is the development of an efficient method for calculating moments-based properties of the voltage response in passive dendritic structures with arbitrary branching. Here we illustrate the method for the particular example depicted in Fig. 10. The model in this example consists of a spherical soma 20 μm in diameter, which is connected to a cylinder 100 μm in length and 2 μm in diameter (cylinder 1). At the end of this cylinder, two identical cylinders (cylinder 2 and 3) are connected, each 100 μm long with a diameter of 1 μm. The point connecting the soma and cylinder 1 is denoted by *s*, and the branchpoint between the three cylinders is denoted *b*. The tips of cylinders 2 and 3 are denoted *a* and *c*, respectively. We will assume uniform membrane properties in this example, with $R_m = 20\ k\Omega cm^2$, $C_m = 1\ \mu F/cm^2$ ($\tau = 20$ ms). Also, $R_i = 100\ \Omega cm$ and points *a* and *c* are sealed ends. From these model parameters, we can calculate the electrical length of each cylinder and its R_∞ (Rall, 1989). Cylinder 1 is 0.1λ long, and with R_∞ of $\sim 318\ M\Omega$. Cylinders 2 and 3 are each $\sim 0.14\lambda$ long with R_∞ of $\sim 900\ M\Omega$. The soma membrane resistance is $\sim 1600\ M\Omega$.

A transient input (I_{in}) is injected at point *a*, the tip of cylinder 2. In Fig. 10, a sample input current is depicted and the voltage responses at the soma and at the points *a*, *b*, and *c* are shown for this input. For calculating the input resistance at this point, we should calculate the input resistance at point *b* of the model consisting of cylinder 1 and the soma, and the input resistance at point *b* of the model consisting of cylinder 3 alone (see the algorithm in Fig. 6). Both values are easy to calculate. Using Eq. 30, where R_L is the soma membrane resistance, we find that the input resistance at point *b* of the model consisting of cylinder 1 and the soma is $1083\ M\Omega$. For calculating the input resistance at point *b* of the model consisting of cylinder 3, $R_L \to \infty$, Eq. 30 becomes $R_{in}(0)/R_\infty = \coth(L)$, and we determine that the input resistance is $6409\ M\Omega$. Using Theorem IV for the zeroth moment, we can calculate the input resistance at point *b* for the model consisting of cylinder 1, the soma, and cylinder 3. This input resistance is $1/(1/1080 + 1/6410)M\Omega = 927\ M\Omega$. Using Eq. 30 for cylinder 2, where $R_L = 927\ M\Omega$, yields the input resistance at point *a*, $920\ M\Omega$.

This procedure for calculating R_{in} is not new (Rall, 1959). Now we calculate the input delay at point *a*, using the input resistances we have just calculated. For calculating the input delay at this point, we should calculate the input resistance and the input delay at point *b* of the model consisting of cylinder 1 and the soma, and the input resistance and the input delay at point *b* of the model consisting of cylinder 3 alone (see the algorithm in Fig. 6). The input resistances were calculated above. Using Eq. 35, where R_L is the soma membrane resistance and D_L is the soma membrane time constant (= 20 ms), we find that the input delay at point *b* of the model consisting of cylinder 1 and the soma is 19.59 ms. For calculating the input delay at point *b* of the model consisting of cylinder 3, $R_L \to \infty$, and Eq. 35 becomes simple, because $\xi = 1$ and $\kappa = 0$. We find that the input delay is 19.87 ms. Using Theorem IV for delays (Eq. 31), we can calculate the input delay at point *b* for the model consisting of cylinder 1, the soma, and cylinder 3. This input

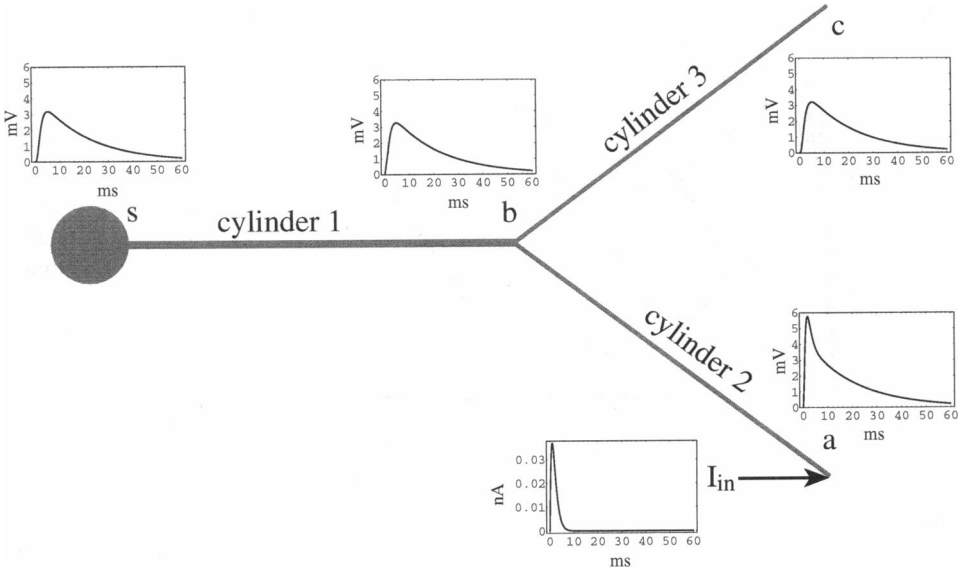

FIGURE 10 Simple model used to illustrate calculation of moments-based properties. A transient current input (I_{in}) is injected at the tip of cylinder 2 (point *a*). The voltage response at points *a, b, c,* and *s* is analyzed in the Discussion. The soma is 20 μm in diameter, all of the cylinders are 100 μm long, the diameter of cylinder 1 is 2 μm, and the diameter of the other cylinders is 1 μm. The membrane is uniform, with $R_m = 20$ kΩcm^2, $C_m = 1$ μF/cm^2 ($\tau = 20$ ms). $R_i = 100$ Ωcm. The sample current shown is $i(t) = 0.1 \cdot t \cdot e^{-t}$, where t is in milliseconds and the current is in nanoamperes. The voltage responses depicted at points *s, a, b,* and *c* refer to this sample current input.

delay is 19.63 ms. Using Eq. 35 for cylinder 2, where $R_L = 927$ MΩ and $D_L = 19.63$ ms, yields the input delay at point *a*, 17.32 ms.

We can continue and calculate the input broadening in the same way, but we will skip this straightforward calculation. Instead, we will calculate the attenuation factor and propagation delay along paths in the model. The input resistance and input delay at point *b* for the model consisting of cylinder 1, the soma, and cylinder 3 are the R_L and D_L for cylinder 2 in Eqs. 29 and 34. We find that the attenuation factor from point *a* to point *b* is 1.15, and the propagation delay is 2.54 ms. From point *b* to point *c*, we use Eqs. 29 and 34 for cylinder 3, where $R_L \rightarrow \infty$, and find that the attenuation factor is 1.01 and the *PD* is 0.2 ms. From point *b* to the soma, we use the same equations, now for cylinder 1, where R_L is the soma membrane resistance and D_L is the soma membrane time constant. The attenuation factor found is 1.02 and the propagation delay is 0.49 ms.

The results were verified by compartmental modeling and found to be very similar. A small difference is due to the inaccuracy of a compartmental model (compartments of 0.01 were used) and the integration time of the compartmental model (the simulation was run until $t = 60$ ms).

An algorithm for trees equivalent to a single cylinder

Many important insights can be obtained from analyzing the family of trees that are equivalent to a single cylinder (Rall 1959, 1962a,b, 1969). Rall and Rinzel (1973) introduced an analytical method to compute the attenuation of steady voltage in such trees, with current injected into only one dendritic branch. This method is based on the superposition property of linear systems. For example, consider the case of a symmetrical dendritic branching with one branch point. An input, I, is injected at the tip of one of the terminals. The voltage response in this case is the sum of two voltage responses: the response in the case where both dendritic terminals receive a current of $I/2$ and the response in the case where one terminal receives a current of $+I/2$ and the other receives a current of $-I/2$ (Rall and Rinzel, 1973). These two responses are easily computed if the tree is symmetric and equivalent to a cylinder. This analysis holds even if I is a transient input. Hence, using the Multi-inputs Theorems (Theorem VI for the various moments-based properties), transient attenuation, delays, broadening, etc., may be analyzed for such "equivalent trees." This superposition method can be extended to higher orders of branching.

The advantage of such an analysis over the general recursive algorithms discussed above is that in these idealized trees, the general dependence of the moments-based parameters on the order of branching and the electrical length may be expressed analytically. This yields better understanding of the effect of branching on the input resistance and the time course of synaptic potentials. For an example, see an analysis of delays in such structures in Agmon-Snir and Segev (1993).

Two new parameters, $\vec{\lambda}_{eff}$ and $\vec{\tau}_{eff}$, and morphoelectrotonic transforms

We have defined two new functional parameters, $\vec{\tau}_{eff}$ and $\vec{\lambda}_{eff}$. These directional parameters extend the functional meaning of the classical parameters, the membrane time constant, τ_m, and space constant, λ, for dendritic trees. Indeed, for an isopotential structure $\vec{\tau}_{eff} = \tau_m$ and for an infinite cylinder, $\vec{\lambda}_{eff} = \lambda$. For a given direction from a point (y) in a tree, the attenuation rate of a steady voltage is inversely proportional to $\vec{\lambda}_{eff}$. One consequence of this is that the modeled tree can be rescaled with respect to $\vec{\lambda}_{eff}$ to obtain a morphoelectrotonic transform of the tree, called an

attenogram, where each unit of distance represents an e-fold attenuation of voltage (Zador et al., 1995). The other parameter, $\vec{\tau}_{eff}$, is the input delay at point y, when the boundary conditions at all other possible directions (excluding the direction of interest) are sealed ends. The ratio $\vec{\lambda}_{eff}/\vec{\tau}_{eff}$ is the velocity of the centroid (delay Theorem III above). Scaling the modeled tree with respect to the velocity provides another type of morphoelectrotonic transform, called a delayogram, where each unit of distance represents a constant propagation delay (Zador et al., 1995).

The concepts of $\vec{\lambda}_{eff}$ and $\vec{\tau}_{eff}$ can be useful also for tapering cylinders and can be generalized for nonlinear membrane models (unpublished results). This generalization may prove useful in analyzing the behavior of transient signals in nonlinear dendritic trees and in axons.

Extension of the results: transient voltage inputs, synaptic conductance changes, and nonlinear membrane properties

The results of the present study are also applicable to the case of a transient voltage input rather than a transient current input. Note, however, that in this case there is no meaning to the input resistance, input delay, input broadening, etc. Hence, the Reciprocity Theorems and Theorems IV of the various properties are not relevant. The other theorems and the algorithms for computing moments-based properties *are* valid for this case.

Although the analysis using the method of moments is mathematically correct only for linear systems, it can be applied, using caution, to conductance change inputs (which are a more realistic model of a synaptic input). In general, when a synaptic conductance change is used to model a synaptic input, the voltage response also depends on the degree of nonlinearity induced by the synaptic input. Nonetheless, as demonstrated by Rinzel and Rall (1974), the linear case may still be a very good approximation when the conductance change is brief compared to the system time constant (e.g., the conductance change associated with the non-NMDA receptors) as well as when the conductance change is small compared to the input conductance at the synaptic site. Moreover, one should note that the properties of the passive spread of voltage from the input point to other regions of the neuron (i.e., attenuation factor, propagation delay, etc.) are independent of the conductance change at the input site.

In the presence of active conductances in the dendritic membrane, the elegant theorems and algorithms of the method of moments would not hold. It is widely accepted today that in many cell types, the dendritic membrane is not purely passive, and in some cases can support active propagation of action potentials (see Regehr and Armstrong, 1994, for a review). Nevertheless, passive analysis of dendritic models is broadly used as a reference case for the detailed nonlinear model and as a first approximation. A few approaches can be used when utilizing the method of moments in modeling dendrites that include nonlinearities. In some cases, the nonlinear membrane can be linearized for small, subthreshold voltage changes (Koch, 1984). We have not extended this approach, but it seems that although mathematically one can get good approximations for the moments-based properties, it might be hard to interpret the results. This is because the response to a monophasic current injection might be biphasic if the linearized membrane includes an inductive component. In some cases, one can find that while the signal is propagating to a known direction, its centroid is decreasing, wrongly interpreted as "going back in time." A second approach is to use numerical methods (e.g., a compartmental model) for computing the moments-based properties of the positive part of the EPSP. The numerical results of the nonlinear model would be then compared to the analytical results from the reference passive model. A third approach is to use the method of moments to get qualitative insights regarding the spatiotemporal integration in a given dendritic model (e.g., a reconstructed cortical pyramidal cell) and the dependence of the spatiotemporal integration on the geometry and the passive properties of the cell. This approach is called "the concept of decision points," and it is demonstrated in Agmon-Snir (1994) and in Agmon-Snir and Segev (1994). The concept of decision points links the results of the elegant passive analysis and the nonlinear interactions between PSPs in the dendrites. The analysis of synchrony requirements at various points at the dendritic tree is an example of such an approach: the results came from a passive analysis, and these results were interpreted as requirements for synchrony for nonlinear interactions (e.g., nonlinear summation of synaptic inputs, activation of a local threshold for an electrical or a chemical process). Although this approach is practically a simplification and an approximation of the real dendritic tree, it might be found to be very useful in many cases. It may be competitive with the compartmental "realistic" modeling, in which many of the parameters are still not known from experiments, and an "educated guess" of their value is used instead.

CONCLUSIONS

The method of moments is a mathematical tool for analyzing transients in passive dendrites. In this paper, we formalize this method in detail. However, the method of moments is *not* just another shortcut for calculating voltage response in passive dendrites. Instead, it is a useful tool for analyzing the computational capabilities and limitations in dendritic trees. We demonstrated it in the discussion by analyzing the multiple-time windows for synaptic integration in dendritic trees. A more detailed analysis of this and many other implementations of the method of moments can be found in Agmon-Snir and Segev (1993) and in Agmon-Snir (1994). In Agmon-Snir (1994), a link is made between the formal analysis of the moments-based properties and the significance of this analysis to our understanding of the compu-

tational capabilities of neurons, using the concept of decision points.

The main advantages of the analysis of moments-based properties are:

1. The generality of the results for any input shape (Theorems I).

2. The applicability of the results for arbitrary dendritic trees. Using Theorems III and V, the results obtained in the analysis of simple structures may be applied easily to much more complicated structures. This is demonstrated in Agmon-Snir and Segev (1993) and in Agmon-Snir (1994). Moreover, the analytic expressions and efficient algorithms may be used for calculating the moments-based properties in arbitrary dendritic structures.

3. The useful interpretations of the moments-based properties for understanding single neuron computation, as discussed above and in Agmon-Snir (1994).

4. The possible use of the method of moments in experiments—as a method for analyzing synaptic inputs and for analyzing electrical properties of neurons. The experimental use of the moments-based properties is discussed in brief in Agmon-Snir (1994).

It should be noted that the method of moments cannot be used to examine the whole time course of the voltage response in the tree. Information about the exact shape of the response is available only when an infinite number of moments are analyzed. However, for most functional purposes, the exact shape of the transient is not important. Indeed, the first few moments of the signal are sufficient for extracting the most interesting information about the signal. In this work, the effectiveness of the signal is given by the zeroth moment (the strength); the characteristic time is given by the centroid, which is defined by the first two moments (zeroth and first moments); and the width of the signal is given by a measure that is based on the first three moments. Adding the third moment, one may obtain information about the asymmetry of the signal, and by using higher moments more information may be found on the shape of the signal. In Agmon-Snir (1994), however, it is demonstrated that the important features of the voltage response can be characterized by using just the first three moments. This result is not surprising. Indeed, we already know from probability theory that the most important information about a distribution is given by the first moments. The fact that the first few moments convey most of the interesting information in the analysis of dendritic transients is a necessary condition for the application of the method of moments. This is because the analysis of moments of higher orders becomes very complicated. Even for the analysis of the width, which requires the first three moments, the resultant expressions are complicated and it could be hard to derive them without a software tool for symbolic algebra.

We hope that the method of moments will become a standard experimental and theoretical tool for analyzing signal processing in dendritic trees. Incorporating it into software tools for analyzing dendrites (e.g., Neuron (Hines, 1989) and Genesis (Wilson et al., 1989)) would provide a simple and efficient way for exploring the role of the biophysical and morphological properties of the dendritic tree in the computational function of the neuron.

APPENDIX

Proving the theorems of the moments-based properties

We start by analyzing derivatives of the logarithm of the Laplace transform at $s = 0$. For a transient signal $f(t)$, we find, using Eqs. 2, 4, 6, 14, and 15,

$$[\ln(\tilde{f}(s))]_{s=0} = \ln(m_{f,0}) = \ln(\hat{s}_f) \tag{A1}$$

$$\left[\frac{\partial \ln(\tilde{f}(s))}{\partial s}\right]_{s=0} = \left[\frac{\partial(\tilde{f}(s))}{\partial s}(\tilde{f}(s))^{-1}\right]_{s=0} = -\hat{t}_f \tag{A2}$$

$$\left[\frac{\partial^2 \ln(\tilde{f}(s))}{\partial s^2}\right]_{s=0} = \hat{w}_f^2 \tag{A3}$$

The input-output relation between a current injection at point y and a voltage response at point x in a passive structure can be described in the Laplace domain by a transfer function $H(s)$. Using Eq. 13, and setting $i(t) = I(y, t)$ and $o(t) = V(x, t)$, we get

$$\ln(H(s)) = \ln(\tilde{o}(s)) - \ln(\tilde{i}(s)) = \ln(\tilde{V}(x, s)) - \ln(\tilde{I}(y, s)) \tag{A4}$$

Using Eqs. A1–A3 and Eq. 15, it is then straightforward to get from Eq. A4,

$$R_{tr}(y, x) \equiv \frac{\hat{s}_v(x)}{\hat{s}_I(y)} = H(0) \tag{A5}$$

$$D_{tr}(y, x) \equiv \hat{t}_v(x) - \hat{t}_I(y) = -\left[\frac{\partial \ln(H(s))}{\partial s}\right]_{s=0} = -\left[\frac{(dH(s)/ds)}{H(s)}\right]_{s=0} \tag{A6}$$

$$B_{tr}(y, s) \equiv \hat{w}_v^2(x) - \hat{w}_I^2(y) = \left[\frac{\partial^2 \ln(H(s))}{\partial s^2}\right]_{s=0} \tag{A7}$$

We see that $R_{tr}(y, x)$, $D_{tr}(y, x)$, and $B_{tr}(y, x)$ are independent of the shape of the transients, and this proves the Shape Invariance Theorems (Theorems I). In particular, $R_{in}(y)$, $D_{in}(y)$, and $B_{in}(y)$ are independent of the shape of the transients, and thus it is easy to see that the Shape Invariance Theorems are also valid for the attenuation factor $A(y, x)$, the propagation delay $PD(y, x)$, and propagation broadening $PB(y, x)$.

The Reciprocity Theorems (Theorems II) are a direct consequence of the reciprocity property of the Laplace transform, which means that the transfer function, $H(s)$, is the same if one injects current at y and records at x, or vice versa. Hence, the transfer resistance, transfer delay, and transfer broadening, as expressed in Eqs. A5–A7, will be the same in both cases.

For proving Theorems III, we will rewrite Eq. 26,

$$\left|\frac{\partial}{\partial x}\ln(\tilde{V}(x, s))\right| = (\vec{\tilde{R}}_{in}(x, s))^{-1} \cdot \vec{r}_i = (\vec{\tilde{R}}_{in}(x, s))^{-1} \cdot \vec{R}_\infty \cdot \vec{\lambda}^{-1} \tag{A8}$$

We analyze the derivatives of $[\vec{\tilde{R}}_{in}(x, s)]^{-1}$ at $s = 0$,

$$[(\vec{\tilde{R}}_{in}(x, s))^{-1}]_{s=0} = (\vec{R}_{in}(x))^{-1} \quad \text{(A9)}$$

$$\left[\frac{\partial}{\partial s}(\vec{\tilde{R}}_{in}(x, s))^{-1}\right]_{s=0} = -\frac{\vec{D}_{in}(x)}{\vec{R}_{in}(x)} \quad \text{(A10)}$$

$$\left[\frac{\partial^2}{\partial s^2}(\vec{\tilde{R}}_{in}(x, s))^{-1}\right]_{s=0} = -\frac{\vec{\eta}(x)}{\vec{R}_{in}(x)} \quad \text{(A11)}$$

Note that $\tilde{R}_{in}$ at point x in a passive structure is equal to $\tilde{V}$ at this point, when a δ-function current input is injected at point x at time 0. That is because $\tilde{V}(x) = \tilde{R}_{in}(x) \cdot \tilde{I}(x)$ and the Laplace transform of a δ-function current is exactly 1.

From Eq. A8, we get the expressions for the attenuation rate, the signal velocity, and the broadening rate, using Eqs. A1–A3, A9–A11,

$$\vec{A}_r(x) = (\vec{R}_{in}(x))^{-1} \cdot \vec{R}_\infty \cdot \vec{\lambda}^{-1} = (\vec{\lambda}_{eff}(x))^{-1} \quad \text{(A12)}$$

$$\vec{\theta}(x) = \frac{\vec{\lambda}_{eff}(x)}{\vec{D}_{in}(x)} = \frac{\vec{\lambda}_{eff}(x)}{\vec{\tau}_{eff}(x)} \quad \text{(A13)}$$

$$\vec{B}_r(x) = \frac{\vec{\eta}(x)}{\vec{\lambda}_{eff}(x)} \quad \text{(A14)}$$

where all of the variables refer to the propagation direction of the signal. We can see that the expressions do not depend on the structure "behind" the signal or on the point of current injection. Hence, we have proved Theorems III.

Rewriting Eq. 25 we get

$$(\vec{\tilde{R}}_{in}(y, s))^{-1} = (\vec{\tilde{R}}_{in,1}(y, s))^{-1} + (\vec{\tilde{R}}_{in,2}(y, s))^{-1} \quad \text{(A15)}$$

From this equation and using Eq. A9–A11, we find that

$$(R_{in}(y))^{-1} = (\vec{R}_{in,1}(y))^{-1} + (\vec{R}_{in,2}(y))^{-1} \quad \text{(A16)}$$

$$\frac{D_{in}(y)}{R_{in}(y)} = \frac{\vec{D}_{in,1}(y)}{\vec{R}_{in,1}(y)} + \frac{\vec{D}_{in,2}(y)}{\vec{R}_{in,2}(y)} \quad \text{(A17)}$$

$$\frac{\eta_{in}(y)}{R_{in}(y)} = \frac{\vec{\eta}_{in,1}(y)}{\vec{R}_{in,1}(y)} + \frac{\vec{\eta}_{in,2}(y)}{\vec{R}_{in,2}(y)} \quad \text{(A18)}$$

Using Eq. A16–A18, it is straightforward to prove Theorems IV. This proof can be applied easily to more than two directions (e.g., a branch point).

The Equivalence Theorem for input/transfer resistance and voltage attenuation is a direct consequence of the fourth and fifth properties of the Laplace-transformed voltage response (Eqs. 23, 24, and 25) when $s = 0$. For proving the Equivalence Theorem for delays, we recall that $\tilde{R}_{in}$ can be computed at any point in a given segment if $\tilde{R}_{in}$ of the structures at its boundaries are given (Eqs. 24 and 25). If the input resistance and the input delay of a structure at the boundary are known, the zeroth and first moments of $\tilde{R}_{in}$ of this structure are also known. Hence, using Eqs. 24 and 25 and their derivatives with respect to s, the zeroth and first moments of $\tilde{R}_{in}$ at any point in the segment can be computed. In other words, we can find the input resistance and input delay at any point along the segment. This is sufficient for calculating input delays and velocities at any point (and any direction) and, thus, for calculating delays along the segments. The same method can be used to prove the Equivalence Theorem for broadening, using the zeroth, first, and second moments.

Theorems VI are a direct consequence of the linearity property of the Laplace-transformed voltage response. It is easy to see, by using Eq. 15, that the moments of the signal also preserve this linearity. The linearity of the zeroth moment yields the proof of the Multi-inputs Theorem for the signal strength; the linearity of the first moment yields the proof of the Multi-inputs Theorem for delays (when substituting the first moment of f by $\hat{s}_f \cdot \hat{i}_f$); similarly, the linearity of the second moment yields the proof of the Multi-inputs Theorem for broadening.

I am very grateful to Idan Segev for guidance, support, encouragement, and insightful ideas during this research. I would like to thank Wilfrid Rall for his helpful comments and advice, Rodney Douglas for providing the morphological data for Fig. 8, and Moshe Rapp for preparing the simulations using Neuron. Special thanks are to Israel Nelken, who showed me an elegant way of simplifying the proofs of the moments-based properties. Other helpful comments were made by Guy Major and William Softky.

This work was supported by grants to Idan Segev from the Office of Naval Research and the US-Israel Bi-national Foundation.

REFERENCES

Abbott, L. F., E. Fahri, and Gutmann, S. 1991. The path integral for dendritic trees. *Biol. Cybern.* 66:49–60.

Agmon-Snir, H. 1994. A novel approach to the analysis of dendritic transients. Ph.D. thesis. Hebrew University of Jerusalem.

Agmon-Snir, H., and I. Segev. 1993. Signal delay and input synchronization in passive dendritic structures. *J. Neurophysiol.* 70:2066–2085.

Agmon-Snir, H., and I. Segev. 1994. Synapses on dendrites: the gain and the loss. *Soc. Neurosci.* 20:891 (Abstr.)

Barrett, J. N., and W. E. Crill. 1974. Influence of dendritic location and membrane properties on the effectiveness of synapses on cat motoneurones. *J. Physiol.* 239:325–345.

Brown, T. H., R. A. Fricke, and D. H. Perkel. 1981. Passive electrical constants in three classes of hippocampal neurons. *J. Neurophysiol.* 46:812–827.

Butz, E. G., and J. D. Cowan. 1974. Transient potentials in dendritic systems of arbitrary geometry. *Biophys. J.* 14:661–689.

Cao, B. J., and L. F. Abbott. 1993. A new computational method for cable theory problems. *Biophys. J.* 64:303–313.

Carnevale, N. T., and D. Johnston. 1982. Electrophysiological characterization of remote chemical synapses. *J. Neurophysiol.* 47:606–621.

Clements, J. D., and S. J. Redman. 1989. Cable properties of cat spinal motoneurones measured by combining voltage clamp, current clamp and intracellular staining. *J. Physiol.* 409:63–87.

Durand, D. 1984. The somatic shunt cable model for neurons. *Biophys. J.* 46:645–653.

Elmore, W. C. 1948. The transient response of damped linear networks with particular regard to wideband amplifiers. *J. Appl. Phys.* 19:55–63.

Fleshman, J. W., I. Segev, and R. E. Burke. 1988. Electrotonic architecture of type-identified α-motoneurons in the cat spinal cord. *J. Neurophysiol.* 60:60–85.

Hines, M. 1989. A program for simulation of nerve equations with branching geometries. *Int. J. Biomed. Comp.* 24:55–68.

Holmes, W. R. 1986. A continuous cable method for determining the transient potential in passive dendritic trees of known geometry. *Biol. Cybern.* 55:115–124.

Horwitz, B. 1981. An analytical method for investigating transient potentials in neurons with branching dendritic trees. *Biophys. J.* 36:155–192.

Jack, J. J. B., D. Noble, and R. W. Tsien. 1983. Electric Current Flow in Excitable Cells. Clarendon, Oxford, England. 518 pp.

Jack, J. J. B., and S. J. Redman. 1971. An electrical description of the motoneurone, and its application to the analysis of synaptic transients. *J. Physiol.* 215:321–352.

Kawato, M. 1984. Cable properties of a neuron model with non-uniform membrane resistivity. *J. Theor. Biol.* 111:149–69.

Kirkwood, P. A. 1979. On the use and interpretation of cross-correlation measurements in the mammalian central nervous system. *J. Neurosci. Methods.* 1:107–132.

Koch, C. 1984. Cable theory in neurons with active, linearized membranes. *Biol. Cybern.* 50:15–33.

Koch, C., and T. Poggio. 1985. A simple algorithm for solving the cable equation in dendritic trees of arbitrary geometry. *J. Neurosci. Methods.* 12:303–315.

Koch, C., T. Poggio, and V. Torre. 1982. Retinal ganglion cells: a functional interpretation of dendritic morphology. *Philos. Trans. R. Soc. Lond.* 298:227–264.

Lin, T., and C. A. Mead. 1984. Signal delay in general RC networks. *IEEE Trans. Computer-Aided Design.* 3:331–349.

Major, G., J. D. Evans, and J. B. Jack. 1993. Solutions for transients in arbitrary branching cables. I. Voltage recording with a somatic shunt. *Biophys. J.* 65:423–449.

Major, G., A. U. Larkman, P. Jonas, B. Sakmann, and J. J. Jack. 1994. Detailed passive cable models of whole-cell recorded CA3 pyramidal neurons in rat hippocampal slices. *J. Neurosci.* 14:4613–4638.

McKenna, T., J. Davis, and S. F. Zornetzer, editors. 1992. Single Neuron Computation. Academic Press, Boston. 644 pp.

Mel, B. W. 1994. Information processing in dendritic trees. *Neural Computation.* 6:1031–1085.

Neff, H. P. 1984. Continuous, and Discrete Linear Systems. Harper & Row, New York. 519 pp.

Nicoll, A., A. Larkman, and C. Blakemore. 1993. Modulation of EPSP shape and efficacy by intrinsic membrane conductances in rat neocortical pyramidal neurons in vitro. *J. Physiol. (Lond.).* 468:693–710.

Nitzan, R., I. Segev, and Y. Yarom. 1990. Voltage behavior along the irregular dendritic structure of morphologically and physiologically characterized vagal motoneurons in the guinea pig. *J. Neurophysiol.* 63:333–346.

Rall, W. 1959. Branching dendritic trees and motoneuron membrane resistivity. *Exp. Neurol.* 1:491–527.

Rall, W. 1960. Membrane potential transients and membrane time constant of motoneurons. *Exp. Neurol.* 2:503–532.

Rall, W. 1962a. Electrophysiology of a dendritic neuron model. *Biophys. J.* 2:145–167.

Rall, W. 1962b. Theory of physiological properties of dendrites. *Ann. N.Y. Acad. Sci.* 96:1071–1092.

Rall, W. 1964. Theoretical significance of dendritic trees for neuronal input-output relations. *In* Neural Theory and Modeling. R. F. Reiss, editor. Stanford University Press, Stanford, CA. 73–94.

Rall, W. 1967. Distinguishing theoretical synaptic potentials computed for different soma-dendritic distributions of synaptic input. *J. Neurophysiol.* 30:1138–1168.

Rall, W. 1969. Time constants and electrotonic length of membrane cylinders and neurons. *Biophys. J.* 9:1483–1508.

Rall, W. 1977. Core conductor theory and cable properties of neurons. *In* Handbook of Physiology, Section 1, The Nervous System. I. Cellular Biology of Neurons. E. R. Kandel, editor. American Physiological Society, Bethesda, MD. 39–97.

Rall, W. 1989. Cable theory for dendritic neurons. *In* Methods in Neuronal Modeling: From Synapses to Networks. C. Koch and I. Segev, editors. MIT Press, Cambridge, MA. 9–62.

Rall, W., R. E. Burke, W. R. Holmes, J. J. B. Jack, S. J. Redman, and I. Segev. 1992. Matching dendritic neuron models to experimental data. *Physiol. Rev.* 72:S159–S186.

Rall, W., R. E. Burke, T. G. Smith, P. G. Nelson, and K. Frank. 1967. Dendritic location of synapses and possible mechanisms for the monosynaptic epsp in motoneurons. *J. Neurophysiol.* 30:1169–1193.

Rall, W., and J. Rinzel. 1973. Branch input resistance and steady attenuation for input to one branch of a dendritic neuron model. *Biophys. J.* 13:648–688.

Rapp, M., I. Segev, and Y. Yarom. 1994. Physiology, morphology and detailed passive models of guinea-pig cerebellar Purkinje cells. *J. Physiol.* 474:101–118.

Redman, S. J. 1973. The attenuation of passively propagating dendritic potentials in a motoneurone cable model. *J. Physiol.* 234:637–664.

Regehr, W. G., and C. M. Armstrong. 1994. Dendritic function. Where does it all begin? *Curr. Biol.* 4:436–439.

Rinzel, J., and W. Rall. 1974. Transient response in a dendritic neuron model for current injected at one branch. *Biophys. J.* 14:759–790.

Rubinstein, J., P. Penfield Jr., and M. A. Horowitz. 1983. Signal delay in RC tree networks. *IEEE Trans. Computer-Aided Design.* 2:202–211.

Segev, I. 1992. Single neurone models: oversimple, complex and reduced. *Trends Neurosci.* 15:414–421.

Segev, I. 1995. Dendritic processing. *In* The Handbook of Brain Theory and Neural Networks. M. A. Arbib, editor. MIT Press, Cambridge, MA. 282–289.

Segev, I., J. W. Fleshman, and R. E. Burke. 1989. Compartmental models of complex neurons. *In* Methods in Neuronal Modeling: From Synapses to Networks. C. Koch and I. Segev, editors. MIT Press, Cambridge, MA. 63–96.

Segev, I., J. Rinzel, and G. M. Shepherd, editors. 1994. The Theoretical Foundation of Dendritic Function: Collected Papers of Wilfrid Rall with Commentaries. MIT Press, Cambridge, MA. 456 pp.

Softky, W. 1994. Sub-millisecond coincidence detection in active dendritic trees. *Neuroscience.* 58:15–41.

Stevens, C. F. 1994. Cooperativity of unreliable neurons. *Curr. Biol.* 4:268–269.

Stratford, K., A. Mason, A. Larkman, G. Major, and J. J. B. Jack. 1989. The modelling of pyramidal neurones in the visual cortex. *In* The Computing Neuron. R. Durbin, C. Miall, and G. Mitchison, editors. Addison-Wesley, Workingham. 296–321.

Tuckwell, H. C. 1988. Introduction to Theoretical Neurobiology. Cambridge University Press, Cambridge, England.

Whitehead, R. R., and J. R. Rosenberg. 1993. On trees as equivalent cables. *Proc. R. Soc. Lond. B.* 252:103–108.

Wilson, M. A., U. S. Bhalla, J. D. Uhley, and J. M. Bower. 1989. GENESIS: a system for simulating neural networks. *In* Advances in Neural Information Processing Systems. D. S. Touretzky, editor. Morgan Kaufmann, San Mateo, CA. 485–492.

Wolfram Research, Inc. 1993. Mathematica, Ver 2.2, Wolfram Research, Inc., Champaign, IL.

Wyatt, J. L. Jr. 1985. Signal delay in RC mesh networks. *IEEE Trans. Circuits Syst.* CAS-32:507–510.

Zador, A., H. Agmon-Snir, and I. Segev. 1995. The morphoelectrotonic transform: a graphical approach to dendritic function. *J. Neurosci.* 15: 1669–1682.